International Collaboration Center
Institute for Materials Research
Tohoku University
ICC-IMR

ICC-IMR FY2016 Activity Report

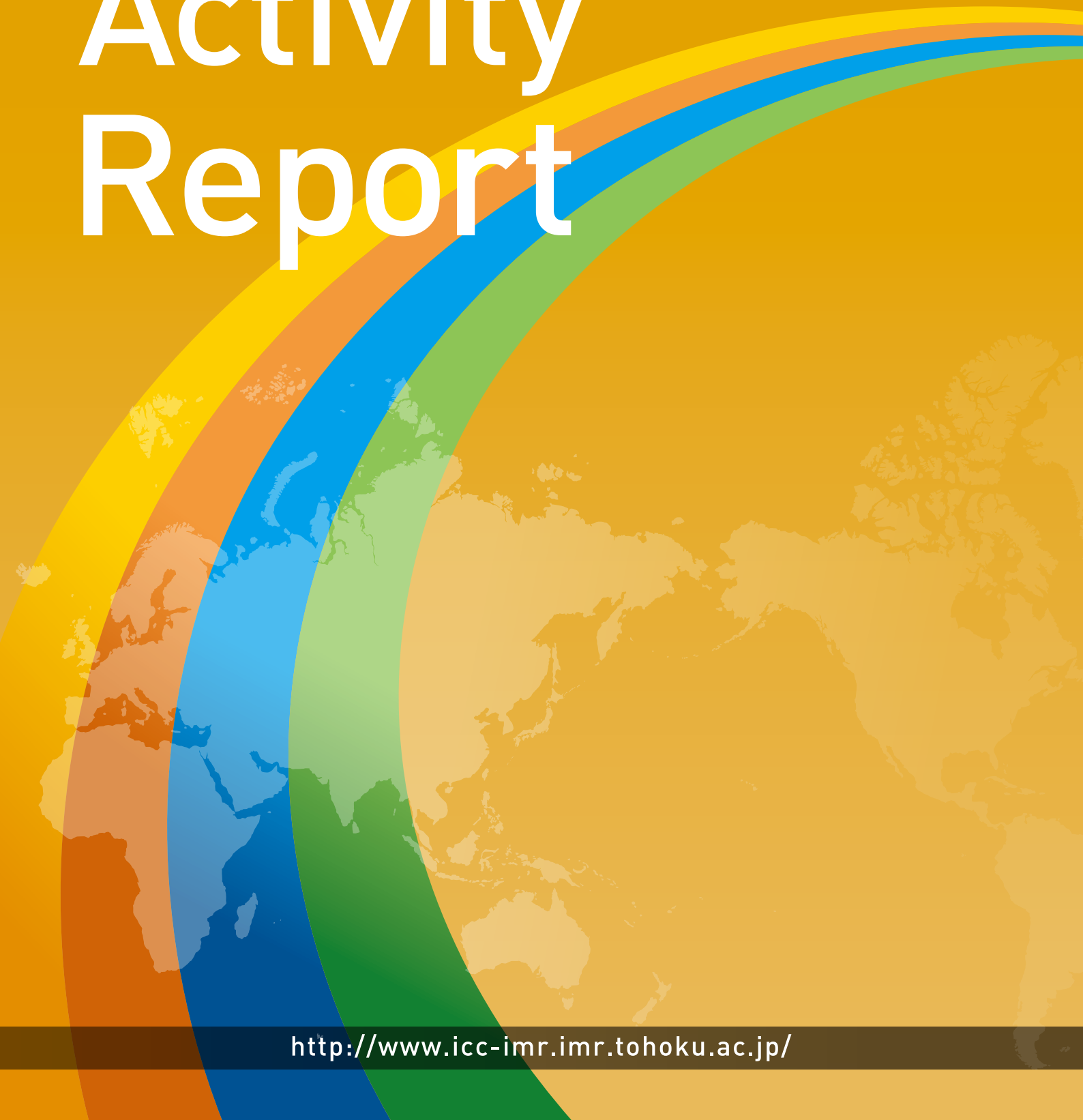

http://www.icc-imr.imr.tohoku.ac.jp/

ICC-IMR FY2016

Activity Report

International Collaboration Center

Institute for Materials Research
Tohoku University

CONTENTS

Preface

It is a great pleasure to present the activity report of the International Collaboration Center of the Institute for Materials Research (ICC-IMR) for the fiscal year from April 2016 to March 2017.

Our core activity is the financial support of application- and peer review-based collaborations with overseas researchers (see next page for details). Here we summarize the fruits of these collaboration in the form of brief summaries written by the leaders of the supported projects in the above period.

On behalf of the committee members of the ICC-IMR (see page 4), I would like to thank all guests and visitors as well as participants in the Schools and Workshops for their contributions to our activities.

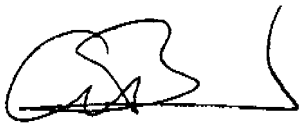

Prof. Gerrit Bauer
Director of ICC-IMR

Mission

The ICC-IMR was founded in April 2008 as the center for international collaboration of the Institute for Materials Research (IMR) a center of excellence in material science, consisting of 27 research groups and five research centers. The ICC-IMR works as a gateway of diverse collaborations between overseas and IMR researchers. The ICC-IMR has invited 49 visiting professors and conducted 23 international research projects since its start-up (please inspect the graph below for more details,). The applications are open to foreign researchers and the projects are evaluated by a peer-review process involving international reviewers.

ICC-IMR coordinates six different programs:

1) International Integrated Project Research

2) Visiting Professorships

3) Short Single Research Visits

4) International Workshops

5) Fellowship for Young Researcher and PhD Student

6) Material Transfer Program

We welcome applicants from around the globe to submit proposals!

Visitors supported by ICC-Programs.

USA	74	Norway	5	Czech Republic	2
China	57	Poland	5	Thailand	2
Germany	51	Taiwan	4	Argentina	1
Korea	43	Spain	4	Austria	1
France	39	Hong-Kong	4	Belgium	1
UK	32	Italy	3	Indonesia	1
Netherlands	17	Mexico	3	Rumania	1
Russia	15	Singapore	3	Slovakia	1
India	8	Australia	3	Turkey	1
Switzerland	7	Denmark	3	Vietnam	1
Iran	6	Slovenia	2		
Canada	6	Ukraine	2		

ICC-IMR COMMITTEE MEMBERS

Director

Prof. Gerrit E. W. BAUER

Steering Committee

Prof. Eiji SAITOH

Prof. Hiroyuki NOJIRI

Prof. Hitoshi MIYASAKA

Prof. Shin-ichi ORIMO

Prof. Akira YOSHIKAWA

Prof. Hidemi KATO

Prof. Masaki FUJITA

Activity Report

Visiting Scholars

FY 2016 Visiting Scholars

No.	Candidate	Host	Proposed Research	Title	Affiliation	Term
16G1	Ilya Sheikin	D. Aoki	Electronic and Superconducting Properties of Ce-Based Heavy-Fermion Compounds with Quasi-Two-Dimensional Fermi Surfaces	Senior Researcher	LNCMI, CNRS, France	2016.4.4-6.3
16G2	Yunping Li	A. Chiba	Influence of Alloying Element on Twinning Boundary Mobility of Mg and Its Alloys	Professor	Central South University, China	2016.7.8-8.9
16G3	Weibin Cui	K. Takanashi	Magnetotransport Properties Caused by the Magnetic Doping in Topological Insulators	Professor	Northeast University, China	2016.7.12-9.1
16G4	Mathias Kläui	E. Saito	Investigation of Insulator Spintronics and the Spin Seebeck Effect in Ferroic Compounds	Director Professor	Johannes Gutenberg University Mainz, Germany	2016.10.6-12.2

Electronic and superconducting properties of Ce-based heavy-fermion compounds with quasi-two-dimensional Fermi surfaces

This research project appeared as a natural continuation of our long-standing collaboration with Prof. D. Aoki. Several new samples of heavy fermion compounds, such as Ce_2RhIn_8 and $CePt_2In_7$, were tested by quantum oscillation and thermodynamic measurements for future experiments in high magnetic fields. In addition, we have finalized the data analysis and discussed some of the previously obtained results. This gave rise, in particular, to a high-level publication related to a drastic change of the Fermi surface across the metamagnetic transition in $CeRh_2Si_2$ [1].

Quantum critical points (QCPs), i.e., continuous phase transitions at zero temperature, play a key role in the physics of heavy fermion (HF) compounds and other materials. Recent theoretical attempts to classify QCPs in HF systems rely on the knowledge of whether the *f* electrons are itinerant or localized on both sides of a QCP, i.e. whether or not they contribute to the Fermi surface (FS). This can be achieved by comparing experimentally established FS topology with the results of band structure calculations performed for both itinerant and localized f electrons. Magnetic quantum oscillations, such as the de Haas-van Alphen (dHvA) effect, are the most direct way to establish the FS topology of a metal.

We have tested and selected several new samples of Ce-based heavy fermion compounds for future high field dHvA measurements. In these materials, such as Ce_2RhIn_8 and $CePt_2In_8$, quantum critical points can be induced by either pressure or high magnetic field. Furthermore, we have finished the analysis and discussion of the results of our previous dHvA measurements in $CeRh_2Si_2$.

The tetragonal HF compound $CeRh_2Si_2$ with a moderate specific heat Sommerfeld coefficient γ = 22.8 mJ/K^2 mol orders antiferromagnetically at T_{N1} = 36 K. Its magnetic structure changes again at T_{N2} = 24 K. When the magnetic field is applied along the crystallographic *c* axis, a complex two-step first-order metamagnetic (MM) transition to a polarized paramagnetic state occurs at about 26 T at low temperatures. Previous low field dHvA measurements suggest that the *f* electrons are localized deep inside the antiferromagnetic phase.

We observed dHvA oscillations both below and above the metamagnetic transition, as shown in Fig. 1 for a magnetic field applied at 2° off the *c* axis. The fast Fourier transform (FFT) spectrum of the dHvA oscillations below the MM transition [Fig. 1 (b)] is dominated by a peak ν at 1.8 kT and its harmonics in good agreement with previous lower field results. We did not observe any dHvA frequencies above 6 kT in the AF state.

Above the MM transition, the amplitude of the dHvA oscillations is much smaller. Nonetheless, two high dHvA frequencies of 8.6 and 16.3 kT are clearly seen in the FFT spectrum [Fig. 1 (c)]. These frequencies are much higher than the frequencies observed below the transition both in our own and previously reported measurements for the same orientation of the magnetic field. This implies a drastic modification of the FS across the MM transition in $CeRh_2Si_2$.

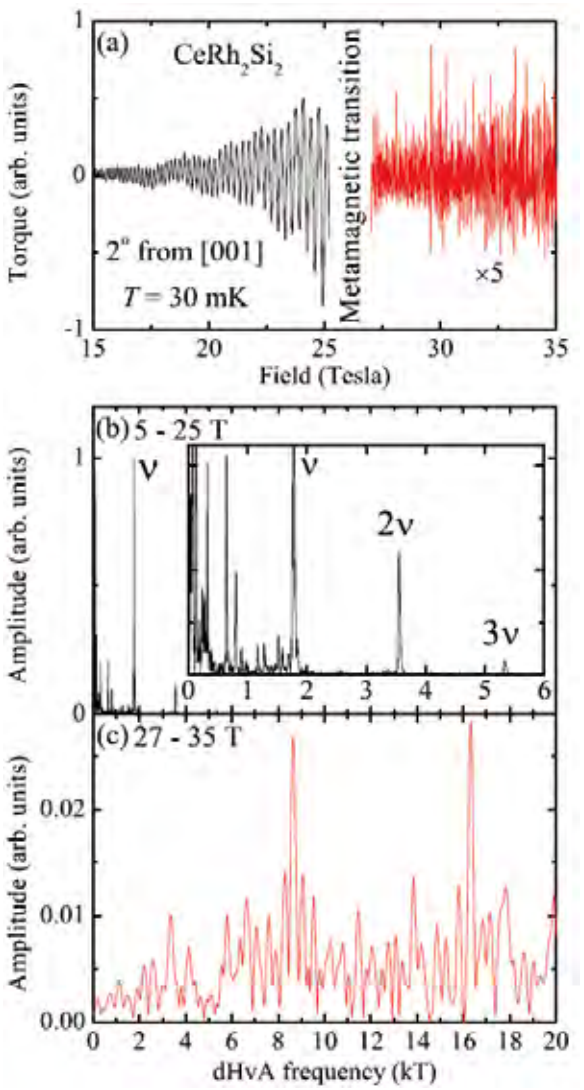

Fig. 1 (a) dHvA oscillations in $CeRh_2Si_2$ and the corresponding FFT spectra (b) below and (c) above the MM transition. The inset shows a zoom of the low frequency part of the FFT spectrum below the transition.

In order to figure out whether the f electrons are itinerant or localized above the MM transition, we compared the experimentally observed angular dependence of the dHvA frequencies with the results of band-structure calculations performed for both CeRh2Si2 (itinerant f electron model) and LaRh2Si2 (localized f electron model). In the latter case, the lattice parameters of CeRh2Si2 were used for the calculations. The calculated FSs are shown in Fig. 2. The comparison strongly suggests that the f electrons remain localized in the polarized paramagnetic state above the MM transition. Rather, a drastic change of the FS is caused by the modification of the Brillouin zone at the MM transition.

The FSs with localized and itinerant f electrons are commonly referred to as “small” and “large,” respectively, as in the latter case the *f* electrons effectively contribute to the FS. The example of the FS reconstruction in $CeRh_2Si_2$ from small to large without delocalization of the *f* electrons emphasizes the ambiguity of the commonly used simplistic conception of “small” and “large” FSs for localized and itinerant *f* electrons, respectively. The FS modification we observe here is different from that reported to occur at the pressure-induced QCP, where the *f* electrons do delocalize and become itinerant.

References

[1] K. Götze, D. Aoki, F. Lévy-Bertrand, H. Harima, and I. Sheikin, Phys. Rev. B **95**, 161107(R) (2017).

.

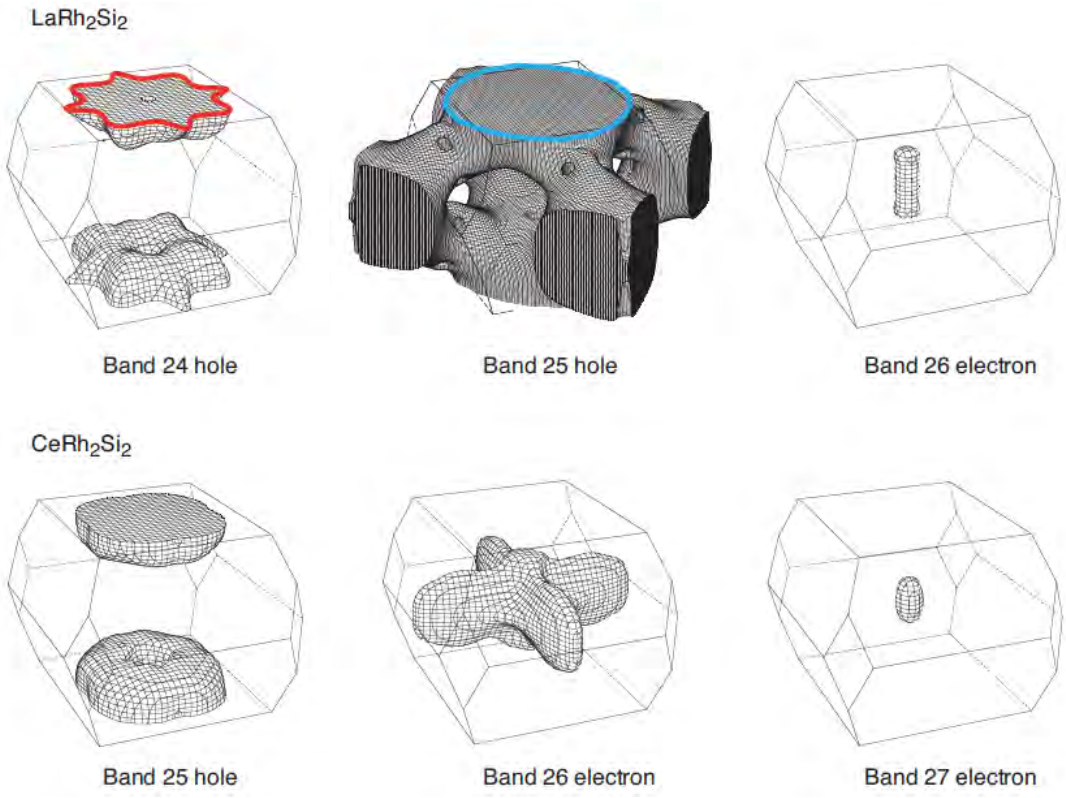

Fig. 2 Calculated Fermi surfaces of $LaRh_2Si_2$ and $CeRh_2Si_2$. For $LaRh_2Si_2$, the orbits giving rise to the experimentally observed high de Haas-van Alphen frequencies are shown.

2 Keywords: heavy fermion, Fermi surface, electronic structure
Dr. Ilya Sheikin (LNCMI-Grenoble, CNRS, Grenoble, France)
E-mail: ilya.sheikin@lncmi.cnrs.fr

Effects of Cu addition on the corrosion behavior of NiCoCrMo alloys in neutral chloride solution

The influence of Cu addition on the corrosion behavior of Ni-30Co-16Cr-15Mo alloy in neutral chloride solution is investigated by electrochemical measurements. The results indicate that alloy with 0.5 mass% Cu shows inferior corrosion resistance compared to Cu-free alloy under open-circuit potential, which is possibly ascribed to the galvanic corrosion from the insufficient coverage of Cu on passive film; higher fraction of Cu exhibits significant improvement on corrosion resistance.

Due to the exceptionally high heat resistance and corrosion resistance, Ni-based alloys are widely used in a variety of severe environments. Among them, Ni-Cr-Mo alloys demonstrate outstanding corrosion resistance, primarily attributed to Cr and Mo elements: Cr promotes the formation of a compact Cr_2O_3 passive film; Mo significantly enhances the localized corrosion resistance by blocking the dissolution of passive film and acts as the effective barrier against the diffusion of ions through the film via precipitating on the external film. Mo (Ⅳ) (as hydrated MoO_2) on the outermost film can be oxidized into Mo (Ⅵ) forming soluble MoO_4^{2-}. The dissolved MoO_4^{2-} anions are cation-selective, resisting the penetration of Cl^- and other ions, which facilitates the growth of inner oxide film.

In spite of the aforementioned merits, the low wear resistance of Ni-Cr-Mo alloy due to the low hardness greatly limits its further application in the injection moulding of fluorine-containing resin or plastic. Recent study indicates that substituting Co for Ni greatly increases the wear resistance of Ni-16Cr-15Mo (NiCrMo) alloy without sacrificing its corrosion resistance to aqueous HF solutions, although with the cost significantly increasing. This can be ascribed to the reduced stacking fault energy (SFE) of alloy by Co addition, leading to higher work hardening on surface during friction. The hardness of Ni-30Co-16Cr-15Mo (NiCoCrMo) alloy can be further enhanced by plastic deformation, although the corrosion resistance of deformed alloy is greatly reduced compared to that of NiCrMo alloy. More recent studies show that further addition of 2 mass% Cu yields a tremendous improvement on corrosion resistance of NiCoCrMo alloy in aqueous HF acid solution, even after severe plastic deformation.

Cu is widely used as an alloying element to enhance the corrosion resistance of alloys in various conditions. For instance, a compact Cu film formed in the alloy/solution interface impedes the dissolutions of alloy elements and dramatically increases the corrosion resistance of AISI304 stainless steel in 30 mass% H_2SO_4 at 50 °C. Similar result by Hong et al. suggests that the passive film of Cu-containing steel mainly consists of Cu compounds in a 10 mass% H_2SO_4 solution. Cu addition alters the passivation from a Mo-dominated into a Cu-dominated passive film in HF solution. Despite the aforementioned efforts devoted to investigate the effect of Cu on corrosion resistance, the effects of Cu addition on the passivation mechanism of NiCoCrMo alloy in common corrosive media such as brine solutions have not been clarified clearly yet. Therefore, in the present research, the influence of Cu addition on the corrosion behavior and passivation mechanism of NiCoCrMo alloys in 3.5 mass% aerated NaCl solution is investigated systematically in detail for the first time.

Electrochemical measurements were conducted to investigate effects of Cu addition's increasing from 0 to 4 mass% on corrosion resistance of Ni-30Co-16Cr-15Mo alloy in neutral chloride solution. Among them, LSV from 300 mV more negative than open-circuit potential (E_{ocp}) up to 1.5 V (vs. saturated calomel electrode, SCE) at a scan rate of 0.167 mV/s were measured. Corresponding results are shown as Fig. 1.

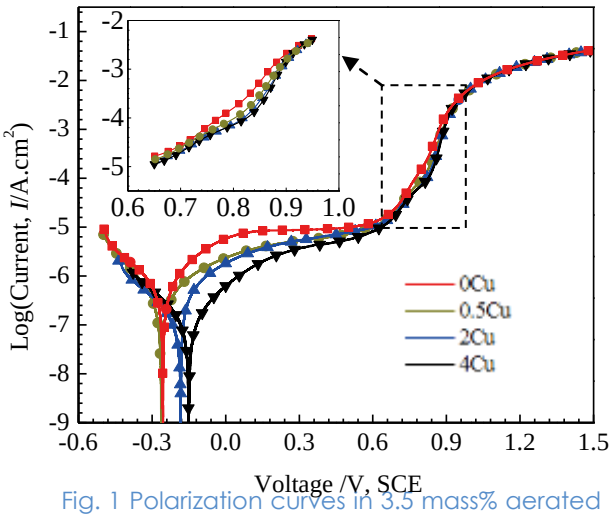

Fig. 1 Polarization curves in 3.5 mass% aerated NaCl solution at room temperature of: 0Cu, 0.5Cu, 2Cu, and 4Cu.

It's obvious that higher fraction of Cu, 4 mass% in this study, exhibits significant improvement on corrosion resistance, with the noblest corrosion potential (E_{corr}) and the lowest corrosion current density (I_{corr}). Moreover, our studies also show slight addition of Cu to Ni-30Co-16Cr-15Mo alloy will be detrimental to alloy's corrosion resistance around E_{ocp}. This is probably related with galvanic corrosion from the insufficient coverage of Cu on passive film.

A new galvanic corrosion model has been set up based on anterior works, to study the effects of Cu content's increasing on corrosion current density. The corrosion galvanic model is shown as Fig. 2. Our theoretical results can be concluded as following equation:

$$(\partial \log \alpha I)/(\partial S_C)=1/((b_a+b_c)*\ln 10)*[((b_a+b_c)*S_C-b_c)/(S_C (S_C-1))]$$

I represent the apparent current density. S_C express cathodic (Cu) area fraction. b_a and b_c stand for Tafel slope for anodic and cathodic reaction.

A maximum for for log I, or I, will occur at $S_C=b_c/(b_a+b_c)$. From above equation, a pronounced tendency can be found that corrosion current density will be increased as Cu content increases firstly from 0, while decreased gradually as S_c exceeds $b_c/(b_a+b_c)$. This is greatly consistent with our experimental results. Sufficient coverage of Cu layer will improve NiCoCrMo alloy's corrosion resistance.

No more discussions are displayed, considering the limitation of space.

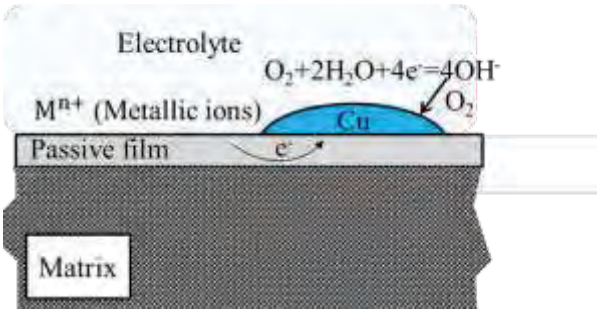

Fig. 2 Schematic illumination of galvanic corrosion on Cu-containing alloys with supposing that Cu will segregate at the outermost surface around open-circuit potential.

The main conclusions are summarized as follows:

Corrosion resistance of the alloys studied is greatly dependent of Cu element. 0.5Cu demonstrates lower corrosion resistance at low potential around E_{ocp}, and improved corrosion resistance at higher potential. The improvement of corrosion resistance becomes more significant with increasing Cu content.

Cr plays a key role in forming the passive film in NiCoCrMo alloys. Meanwhile, the presence of Cu will hinder the extensive dissolution of Cr, ascribed to the rapid formation of a Cu-rich layer on the outmost Cr_2O_3 oxide film. Mo exerts its role by hindering the dissolution of metals by segregating to the surface in transpassive region.

References

[1] X.Y. Wang, Y.P. Li, Y.H. Hou, H.K. Bian, Y. Koizumi, A. Chiba, Mater Sci. Eng. C 64 (2016) **260-268**.

[2] H.K. Bian, Y.P. Li, D.X. Wei, Y.J. Cui, F.L. Wang, S.H. Sun, K. Yamanaka, Y. Koizumi, A. Chiba, Mater Design, 112 (2016) 1-10

Keywords: alloy; corrosion; passivation;

Yunping Li (School of Materials Science and Engineering, Central South University, Changsha, China)
E-mail: lyping@csu.edu.cn
http://mse.csu.edu.cn/

2

Magnetotransport Properties Caused by the Magnetic Doping in Topological Insulators

Well crystallized Cu-doped (Pb,Sn)Se nanocrystalline were prepared by hydrothermal synthesis. More Cu doping content caused the refined grains. Weak ferromagnetism was found due to the Cu doping. The atomic moments per Cu was decreased with increased Cu content. By fitting the temperature-dependent resistivity curve, the energy barrier for electron jumping is also found to decrease. Higher magnetic field delocalizes the electrons, which results into lower energy barrier. At low temperature, the gradually changed field-dependent resistivity showed that the trivial state was even maintained at low temperature in these two samples without any transition into nontrivial state.

The samples with nominal composition of $Cu_x(Pb_{0.77}Sn_{0.23})_{1-x}Se$ (x = 0.05, 0.1) was prepared by hydrothermal synthesis by using appropriate $Pb(CH3COO)_2{\cdot}3H_2O$, $SnCl_2{\cdot}2H_2O$, $CuSO_4{\cdot}5H_2O$, Se powder as Pb, Sn, Cu and Se sources respectively. The hydrothermal synthesizes were carried out at 180ºC for 10 hours. The resultant powders were dried by de-ioned water and ethanol

From the XRD results (Fig. 1), The PbSe-type cubic structure is achieved in both two samples. While, additional peaks from Se impurity phases are observed. The increased width of diffraction peaks indicates that increased Cu content leads to refined grains. By cooling down to 4 K under 0.1 T, the magnetizations are firstly increased slowly in the temperature between 300K and 50 K. when the temperature is decreased further, the magnetization increases drastically without showing any tendency of saturation. The magnetic hysteresis loops of two samples are compared in Fig. 1c. With increased external field, the magnetizations of two samples are increased but not saturated even at 5 T. The “S” shape loop suggests the weak ferromagnetism, which is supposed to be caused by Cu. Defining the magnetization at 5 T as the saturation magnetization (M_s), higher Cu content leads into larger M_s. The atomic moments calculated by Ms are $0.02\mu_B$/Cu for x=0.05 and $0.013\mu_B$/Cu for x = 0.1. Increased Cu content leads into decreased atomic moment per Cu atom. More Cu content leads into closer interatomic distance and stronger coupling, which causes the decreased atomic moment.

Due to the weak ferromagnetism introduced by Cu, the splitted electron energy bands would lead into different transport properties. The resistivities (R) of $Cu_x(Pb_{0.77}Sn_{0.23})_{1-x}Se$ (x = 0.05, 0.1) are measured between 4 K and 300K under zero field and 9 T. the typical semiconducting-like temperature dependences are observed.

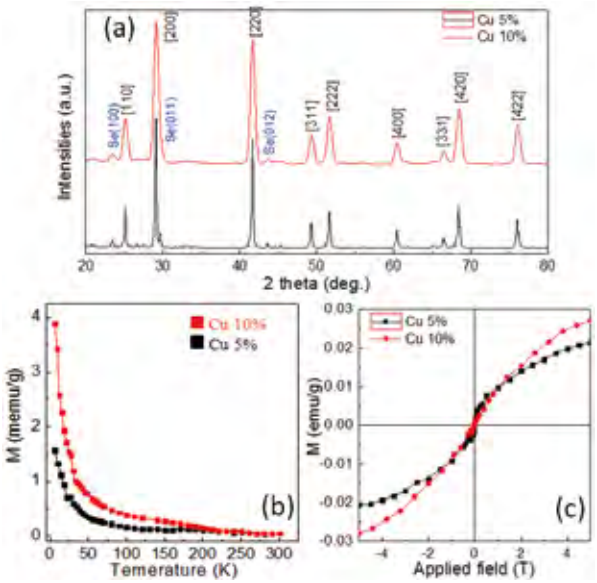

Fig.1 (a) Typical X-ray diffraction patterns of $Cu_x(Pb_{0.77}Sn_{0.23})_{1-x}Te$ (x = 0.05, 0.1). (b) The thermal magnetizations measured under 0.1 T in a cooling process. (c) The magnetic hysteresis loops measured at 4 K.

By applying 9 T, the dependences are not changed. By exponential fitting the R-T curves, the energy barrier is calculated to be 1.69 K_BT for zero field and increased to 3.21 k_BT for 9 T in $Cu_{0.05}(Pb_{0.77}Sn_{0.23})_{0.95}Se$. The increased energy barrier indicates that the electron is inclined to be localized. Only increasing Cu content, the energy barrier is decreased to 0.89 k_BT under zero field and 3.04 k_BT under 9 T. The change of the energy barrier with increased Cu doping is also due to the stronger exchange coupling. Higher Cu concentration leads into closer interatomic distance, which facilitates the tunneling of electrons between Cu atoms.

Fig. 2c and Fig. 2d show the magneto-conductance changes as the function of applied field. At 2K, an upward cusp is observed in ΔG-T curve. With increasing temperature, the cusp become curved and gradually changed into "W" shape. As comparison, with higher Cu content, the similar upward cusp is observed for ΔG-T curve at 2 K. With elevated temperature, the sharp corn becomes broadened. By comparing with R-T curve in Ref. 1, the trivial state is confirmed in the case of x=0.05. With increasing Cu content, the disappeared W-shape R-H curves and the appeared broadened R-H curve near zero field suggest the possible non-trivial state. while further confirmation is necessary by using APPERS to examine the temperature-dependent electron band changes.

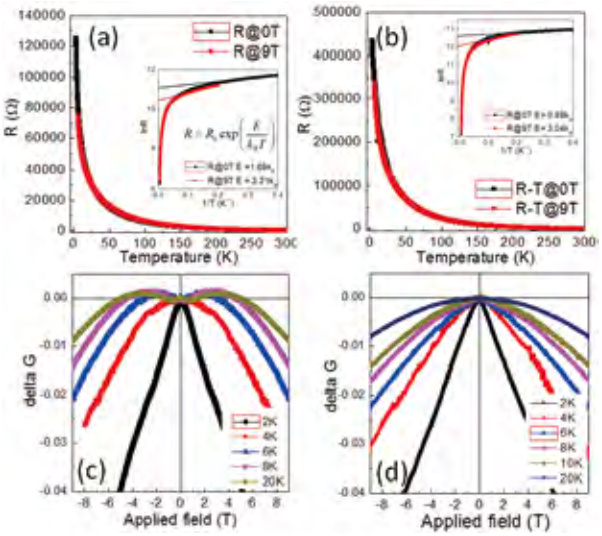

Fig.2 The temperature-dependent resistivity of $Cu_x(Pb_{0.77}Sn_{0.23})_{1-x}Te$ (x = 0.05(a), 0.1(b)) under zero field (black) and 9 T(red). The conductance change as the function of applied field for $Cu_x(Pb_{0.77}Sn_{0.23})_{1-x}Te$ (x = 0.05(c), 0.1(d)) at various temperature.

References

1. M. Safdar et al, Nano Lett. 2015, 15, 2485−2490
2. X. Q. Zhou, W. B. Cui* et al, J. Magn. Magn. Mater., accepted.

Keywords: magnetoresistance (magnetic); electronic structure;
Full Name: Weibin Cui
E-mail: wbcui2014@outlook.com;
http://english.neu.edu.cn/key4.html#

Investigation of Insulator Spintronics and the Spin Seebeck Effect in Ferroic Compounds

Information transport and processing by pure magnonic spin currents in insulators is a promising alternative to conventional charge-current driven spintronic devices. The absence of Joule heating as well as the reduced spin wave damping in insulating ferromagnets has been suggested to enable the implementation of efficient logic devices. During the stay at ICC-IMR, magnetization orientation dependent spin signal detection in collinear magnetic multilayers with spin transport by magnonic spin currents was studied. We found in $Y_3Fe_5O_{12}$ | CoO | Co tri-layers that the detected spin signal depends on the relative alignment of $Y_3Fe_5O_{12}$ and Co. This demonstrates a spin valve behavior with an effect amplitude of 125% in our systems. Furthermore we also worked on topological spin structures leading to a joint high impact publication.

In Fig. 1 (a) the YIG/CoO/Co multilayer sample is schematically shown [1]. After determining the switching properties of both YIG and Co, we study next the measured spin signal as a function of alignment of the YIG and Co layer. Fig. 1c-f shows field-dependent voltage signals generated in sample A at T = 120K induced by f = 4.5 GHz microwave irradiation. By the application of specific field sweep sequences, parallel (d, e) as well as anti-parallel (c, f) alignment of YIG and Co is realized. In the parallel state (Fig. 1d,e) a multi-peak voltage signal appears. It is well fitted by two overlapping Lorentzian line shapes of opposite sign, slightly shifted peak fields, and different line widths. The antiparallel state (Fig. 1c,f), on the other hand, exhibits a voltage peak of one polarity but with a significant asymmetry, which can be fitted by two overlapping Lorentzian functions. The comparison of all four datasets allows us to both separate and attribute the peaks to different effects. Depending on the individual orientation of YIG and Co, the peaks change sign separately and thus can be identified as (i) the signal of the spin current generated by spin pumping from the YIG, transmitted across the CoO and detected by the ISHE in the Co (blue curves in Fig. 1c-f) and (ii) a second signal that depends only on the Co layer direction and thus originates from the Co (green curves in Fig. 1c-f). For the latter possible explanations are a thermally induced ANE signal or spin rectification (SR).

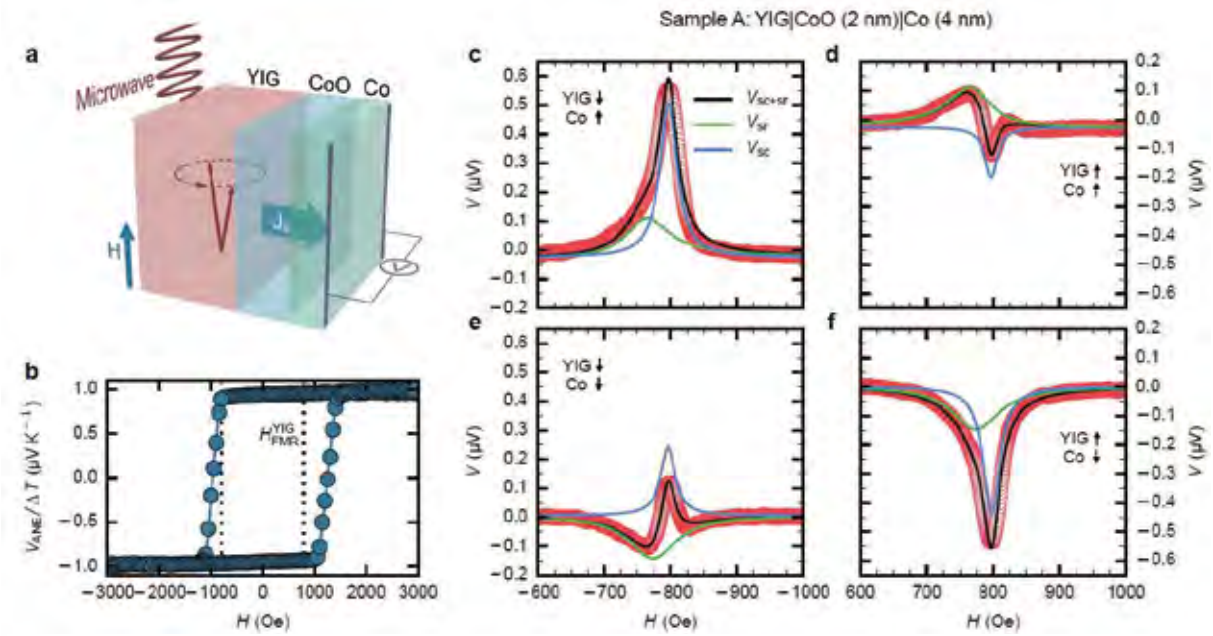

Fig. 1 (a) Illustration of the investigated YIG | CoO | Co tri-layer system. A spin current J_s induced in the YIG by FMR spin pumping propagates through the CoO intermediate layer and is detected electrically in the Co layer via the ISHE. The relative magnetization orientation of YIG and Co can be adjusted to be either parallel or antiparallel. (b) Typical ANE hysteresis loop observed at T = 120 K, being field cooled at H_{ext} = 90 kOe. (d)-(f) Field-dependent voltage signals detected in sample A induced by microwave irradiation. The total signal is given by a superposition of two distinct signals V_{sc} and V_{sr}, the sign of which individually depend on the YIG respectively the Co orientation. The amplitude of V_{sc} furthermore depends on the relative alignment of YIG and Co. **(from [1])**

The intriguing discovery in this experiment is the alignment-dependent amplitude of V_{sc} analogous to the spin-polarized charge current transmission in a conventional spin valve. Whereas V_{sr} is not depending on the relative alignment of the layers, the amplitude of V_{sc} is nearly twice as large in the antiparallel alignment state as compared to the parallel state.

The alignment-dependent spin current transport signal amplitude now naturally lends itself to the implementation of a magnon spin valve effect. Comparing the amplitude of V_{sc} for parallel and antiparallel alignment in Fig. 1, we find an amplitude of the magnon spin valve effect of 120%. To check the reliability of the magnon spin valve effect, the magnetization direction of the Co top layer is switched several times in a row and the voltage response towards the applied microwave is recorded. Since in typical application schemes the external field is fixed instead of being swept and thus one voltage level is probed instead of acquiring the whole absorption spectrum, we choose a single fixed field value at which we acquire the signal amplitude. We find a large difference in the signal difference of the total voltage for parallel and antiparallel alignment. We find for instance in Fig. 1 for the sample an absolute voltage difference of 408 nV and a total spin valve effect amplitude of 290%.

In conclusion of this part of the work, we demonstrated the magnon spin valve effect in YIG | CoO | Co multilayers by showing that the spin current transmission signal amplitudes depend on the relative alignment of YIG and Co. The total voltage signal measured includes two contributions whose signs depend individually on the YIG and Co magnetization directions and thus yield different signal amplitudes and signs. This enables one to encode even two bits of information in the magnetic configuration of the spin valve. The presented setup gives a new insight into spin-dependent transport effects in ferromagnetic metals and provides a missing switch component for magnon-based applications thus making the work a key step towards further magnon-based logic gate operation.

Finally in addition to this work, we also studied topological spin structures by a combination of numerical simulations [2] and experimental work [3].
Magnetic skyrmions are promising candidates for future spintronic applications such as skyrmion racetrack memories and logic devices. They exhibit exotic and complex dynamics governed by topology and are less influenced by defects, such as edge roughness, than conventionally used domain walls. In particular, their non-zero topological charge leads to a predicted ‘skyrmion Hall effect’, in which current-driven skyrmions acquire a transverse velocity component analogous to charged particles in the conventional Hall effect. Here, we use nanoscale pump–probe imaging to reveal the real-time dynamics of skyrmions driven by current-induced spin–orbit torques. We find that skyrmions move at a well-defined angle that can exceed 30 degrees with respect to the current flow. In contrast to conventional theoretical expectations, this skyrmion Hall angle increases linearly with velocity. We qualitatively explain our observation based on internal mode excitations in combination with a field-like spin–orbit torque, showing that one must go beyond the usual rigid skyrmion description to understand the dynamics.

Keywords: spin current,spin wave,spintronics
Mathias Kläui (Johannes Gutenberg University Mainz)
E-mail: klaeui.mathias.michael.a8@tohoku.ac.jp
http://www.imr.tohoku.ac.jp/ index.html

References

[1] J. Cramer et al., (in preparation)
[2] A. de Lucia et al., Phys. Rev. B 94, 184415 (2016)
[3] K. Litzius et al., Nature Phys. 13, 170 (2017)

Activity Report

Integrated Projects

FY2015-2016 Integrated Projects

No.	PI	Host	Proposed Research	Title	Affiliation	Term
15PJT2	Martin Nikl	A. Yoshikawa	Development of the Next Generation Detector for High Energy Physics	Professor	Institute of Physics, Czech Academy of Sciences (CAS)	FY2015-2016
15PJT3	Pascal Manuel	H. Nojiri	Investigation of Magnetic and Charge Dynamics by Combining Pulsed Neutron-X-ray Sources and Pulsed High Magnetic Fields	Senior Researcher	ISIS Pulsed Neutron and Muon Facility, STFC Rutherford Appleton Laboratory	FY2015-2016

Integrated Project: Development of the Next Generation Detector for High Energy Physics

The next-generation detectors for high energy physics experiment including ILC and hadronic detector have triggered the search for novel scintillating materials. Therefore we have developed a new fiber scintillator with a fine spatial resolution and good light output in this project using a micro pulling down method and also other methods.

The Standard Model of particle physics is a theory unifying the electromagnetic, weak and strong interactions, as well as classifying all the known subatomic particles. Later, Prof. S. Sakata, Prof. M. Kobayashi, Prof. H. Masukawa and other Japanese researchers significantly contributed to this model. Although this model assumes that neutrino mass is zero, Japanese and other researchers found the evidence of the neutrino mass related to the neutrino oscillation. Moreover, we cannot describe dark matter by this model up to now. Thus, new theory should be developed, especially with focus on the description of weak interaction.

New theories have emerged recently, such as Supersymmetric theory, extra dimensions theory and so on, however, their experimental proof is missing.

The particle identification, which means to discriminate generated particle such as pion, proton, neutron, electron and others at the moment of the collision, is important to evaluate the collision event. At this collision event, we can find new physics or new particle. The position-sensitive detector can be used for the particle identification.

For position–sensitive detectors fiber type scintillators can be used. The candidates for the new materials are inorganic crystals such as oxides due to their higher radiation hardness when compared o organic materials such as plastic ones which are usually used in the form of fibers for high energy physics experiments [1, 2].

Our ICC-IMR teams including IMR/Tohoku University are members of “Intelligentsia supporting world-famous research institute to develop next-generation particle detectors” project (INTELUM) which is one of the CERN-coordinated projects with focus on development of the next-generation detectors for high energy physics experiment including ILC and hadronic detector. In this project, we develop a new fiber scintillator with a fine spatial resolution and good light output using our original crystal growth technique: the micro-pulling-down method [3].

The final purpose of the ICC-IMR project is to search for new scintillation materials and to develop the fiber crystal growth technology for a position-sensitive calorimeter (particle tracking detector) to detect generated particles from electron-positron collisions in the ILC project. Moreover, these materials can be applied to the next-generation hadron colliders (hadron-hadron collisions, post LHC).

Our Team members from Institute of Physics /Czech Academy of Sciences, University of Milano-Bicocca (Italy), General Physics, Institute of Russian Academy of Sciences, Université Claude Bernard Lyon 1 (France) and IMR/Tohoku University, and most of our members join INTELUM project.

We grew several inorganic fibers such as RE-doped CaF_2, RE:$(Gd, Lu)_3(Ga, Al)_5O_{12}$, RE:$(Gd, La)_2Si_2O_7$ by the micro-pulling down method as shown in Fig.1., where RE are rear-earths such as Ce or Nd.

After, the the light outputs and decay times of the cut and/or polished samples were evaluated in IMR/Tohoku Univ. To evaluate the scintillation properties, we have developed and assembled some photon detector systems using Si-based diodes (i.e. Si-avalanche photo-diode, Si-photo-multiplier) and circuits such as a pre-amplifier, shaper, etc. (Fig. 2).

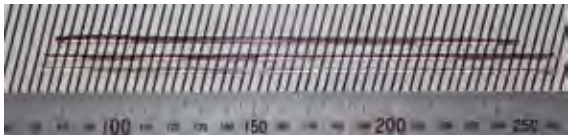

Fig.1 Photograph of fiber scintillator.

Moreover, we showed that some materials co-doped with Mg or other alkali metals have shorter decay times, and radiation hardness of some samples was improved [4]. Thus, Ce: $(Gd, Lu)_3(Ga, Al)_5O_{12}$, Ce:$(Gd, La)_2Si_2O_7$ codoped with Mg or other metals were also grown and their scintillation properties were investigated.

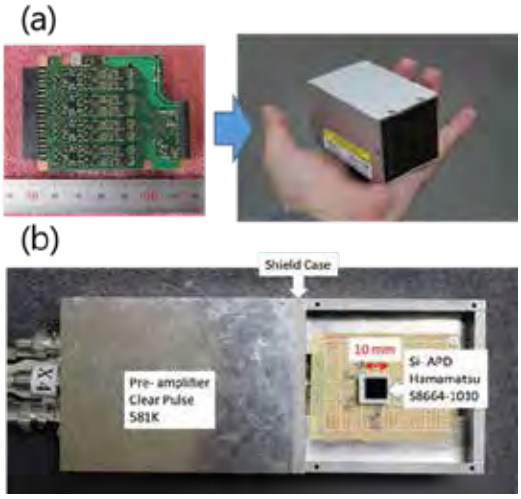

Fig. 2 photograph of evaluation system for light outputs, energy resolution: Si-Photo Multiplier (a) and Si-Avalanche photodiode (b)

Additionally, 1-cm long fiber samples of Ce/Mg:$Lu_3Al_5O_{12}$ and Ce/Mg:$Y_3Al_5O_{12}$ with 3x3 mm^2 cross-section or 3 mm diameter with Mg concentration 0, 3,000 and 6,000 ppm prepared in Tohoku University were supplied to CERN and Czech team. They also tested the scintillation properties such as light output or decay time.

Up to now, we succeeded in growing several fibers with good light outputs of over 30,000 photons/MeV, fast decay time of 40 – 90 ns and good radiation hardness of over 1 Gy/h for some samples, which means that the goal of the ICC-IMR project were achieved. Thus, our results have supported INTELUM activities, and our teams could play a very important role in the INTELUM.

As for the next steps, we grow longer fiber with a length of over 200 mm in order to use it in the experiment. The photon-self-absorption is one of the big issues for such a long fiber. Thus, we studyied how to suppress the photon-self-absorption. We suppose to find the candidate material for the next-generation experiment by 2019 at the latest, therefore we continue the searching the novel materials.

Appendix and acknowledgement

Regarding the ICC-IMR project and INTELUM projects, over 10 foreign researchers have visited in Sendai in the past 2 years, while 9 Japanese researchers including 5 students visited collaborating laboratories such as CERN, Institute of Physics /Czech Academy of Sciences, University of Milano-Bicocca and Université Claude Bernard Lyon 1. Additionally, INTELUM meeting was held in Sendai in 2016. Travel expenses of some researcher were supported by this ICC-IMR project. Moreover, we have published several papers [5-8] regarding as this project.

References

[1]. https://twiki.cern.ch/twiki/bin/view/LHCb/UpgradeSciFiTracker
[2]. Tobin, Mark, Nucl. Inst. and Meth. in Phys. Res, A, 824, p. 148-151 (2016).
[3]. A. Yoshikawa et al., Opt. Mater. 30, pp..6-10 (2007).
[4]. M. Nikl et al., Cryst. Growth Des., 14 (9), pp 4827–4833 (2014,)
[5]. T. Horiai, A. Yoshikawa et al. Opt. Mat. Vol. 65 pp. 56 - 59 (2017)
[6]. S. Kurosawa, A. Yoshikawa et al., J. Mater. Sci., accepted
[7]. S. Kurosawa, A. Yoshikawa et al., JINST 12, C02042 (2017).
[8]. T. Horiai, A. Yoshikawa et al., Opt. Mat. Accepted.

Keywords: crystal growth, optical properties
Akira Yoshikawa (Advanced Crystal Engineering)
E-mail: yoshikawa@imr.tohoku.ac.jp
http://yoshikawa-lab.imr.tohoku.ac.jp/

Investigation of Magnetic and Charge Dynamics by combining Pulsed Neutron-X-ray sources and Pulsed High Magnetic Fields

High magnetic field scattering experiments have been conducted by using a compact pulsed field generator developed at IMR. Experiments have been successfully performed on 5f-itinerant intermetallics, multiferroic transition metal oxides and high T_c-superconductors. The determinations of the order parameters and related wave vectors as well as lattice symmetries have been conducted, which shows the usefulness of such scattering experiments in high magnetic fields.

1. Introduction

A high magnetic field induces interesting new phases of matters by its strong coupling with spin, charge and lattice degrees of freedom of correlated electrons. To investigate such exotic states, the use of neutron and X-ray scatterings are indispensable because magnetic, charge and lattice order parameters can be determined directly in these methods. The combinations with high magnetic fields, however, have been quite rare for the complexity of experimental set up and for the limited maximum field in superconducting magnets.

To breakthrough this situation, in this project, we have developed compact pulsed field generators to conduct neutron and X-ray scattering experiments in very strong magnetic fields of 20-50 T. These have been used to in experiments on various materials in oversea and domestic facilities. The developed systems have been permanently installed in two facilities, ISIS spallation neutron source in UK and X-ray free electron laser source at Stanford linear accelerator laboratory in USA. Moreover, a mobile capacitor bank which can be shared among other facilities by the international collaboration with ICC-IMR is also manufactured.

2. Outline of the generator

Figure 1 shows the mobile capacitor bank designed and assembled at IMR. It stores 16 kJ energy and can drive different mini coils tor X-ray spectroscopies and X-ray diffraction. For the X-ray diffraction, 33 T is available with a split-pair magnet. For hard X-ray absorption spectroscopy, the maximum magnetic field of 50 T is available with a solenoid coil of 3 mm bore. In neutron diffraction, 30 T and 40 T magnet inserts are developed. A compact 60 kJ capacitor bank is used for 40 T neutron insert. The photo in Fig.1 shows the 30 T magnet for neutron diffraction.

On of the most important features of the pulse magnetic field is the flexible design of magnets, which is essential to compromise the critical requirements in the highest possible level. Such ability is the important basis of the successful applications. For example, our pulsed magnet has been also used to explore unknown elementary particle called axion, which is believed to be responsible for dark matter in the space. In high magnetic fields, the high flux X-ray should converts into axion with higher efficiency. By the collaboration with Tokyo University group, we have succeeded in narrowing the area of the possible axion energy[1]. As such, the combination of strong magnetic fields and neutron and X-ray opens the new scientific area in both condensed matter and in fundamental physics. In the following, we present a few examples of scattering experiments.

Fig. 1The mobile pulsed field generator and the magnet used for neutron diffraction.

3. Neutron diffraction

The first example is the study of magnetic field induced ordering in URu_2Si_2 with tetragonal unit cell. This compound has attracted interests in many years for the appearance of the mysterious hidden order phase, where no clear order parameter has been identified although the evidence of the phase transition is shown by the macroscopic measurement such as heat capacity. In the magnetic fields of 30-40 T, this hidden order is destroyed and some magnetic order seems to appear. For the lack of the neutron diffraction, the related magnetic structure has not been known over 30 years.

By the series of experiments at ILL and at ISIS, we have found that the magnetic structures of the high field phases are sensitive to the doping.

Namely, a commensurate up-up-down type order appears in the tetragonal plane when 4 % of Ru is replaced with Rh. This commensurate order disappears when Rh doping is reduced to 2 % and then an incommensurate density wave like magnetic phase is found in pure compound[2]. This observation indicates that the magnetic field induced transition is closely related with the Fermi surface structure and its nesting. Such unique information cannot be obtained without neutron diffraction.

The second example is the magnetoelectric Lithium orthophosphate $LiNiPO_4$. The application of a magnetic field along the crystallographic *c*-axis causes the electrical polarization $\boldsymbol{P}=\alpha\boldsymbol{H}$ along the *a*-axis. The magnetoelectric coefficient is among the largest in transition metal compounds. Motivated by pulsed-field magnetization and electric polarization measurements up to 55 T, we have engaged in a campaign to determine the characteristic propagation vectors of the magnetic phases for high magnetic fields[3].

One of the present highlight is the neutron diffraction at 41.2 T with which we could determine that the phase VII appearing above 39 T is commensurate and the phase VI appearing in 37-39 T is incommensurate. To the best of our knowledge, this is the highest magnetic field ever employed in neutron diffraction experiment. With the present results, we confirmed that all magnetoeelectric phases are commensurate, while all non-polar phase is incommensurate in $LiNiPO_4$. Such universal behavior can be only known by the neutron diffractions in the wide range of magnetic field.

In our experiment, we successfully employed the pulsed field Laue diffraction technique and managed to determine the magnetic propagation vectors of all magnetic phases of interest. It seems certain that pulsed field Laue diffraction will become an increasingly important part of the neutron scattering toolbox, and that many exciting high-field magnetic phases in a diverse range of material classes are now within reach. From a technical perspective, increases of the maximum field are feasible, and further improvements of neutron instrumentation and beam power will guarantee the future success of pulsed-field Laue diffraction.

4. X-ray Diffraction

One of the recent highlights of X-ray diffraction is the observation of unidirectional and three -dimensionally correlated charge density wave(CDW) in magnetic fields above the upper critical fields. The CDW states appearing in Cu-oxide superconductors have been intensively studied. However, the direct observation of the CDW super-lattice peak had been made only in magnetic fields had been desired for long time.

We combined two pulsed tools, the pulsed magnet and the pulsed X-ray source to accomplish this difficult task. The magnetism division of IMR has developed an extremely compact split-pair magnet generating magnetic fields over 30 T. The bore of the coil is only 3 mm and the length of the coil is as short as 25 mm. The Stanford Laboratory offers the most intense pulsed laser source on the earth. When these two tools are combined, weak CDW peaks in $YBa_2Cu_3O_{6.67}$ can be detected clearly in a single shot pulsed magnetic field.

In the present experiments, a new CDW state with strong three-dimensional correlation is discovered. The index of this CDW state is given by (δ, 0, *l*), where δ is related to the localized charge modulation in the *c*-plane. Moreover the index *l* is found to be an integer. This unique feature shows a sharp contrast to the two-dimensional CDW peak found in lower magnetic fields at (δ, 0, *l*/2) position, where the modulation pitch along the *c*-axis is doubled. The intensity of *l*=integer peak grows rapidly in high magnetic fields, while that of the half-integer peak saturates in lower fields. The appearance of a state with localized electrons with strong three-dimensional correlation shows the essential role of the strong electron correlation in the normal state of $YBa_2Cu_3O_{6.67}$[4, 5]. The observation of the weak super lattice peak shows the possible detection of the Fermi surface nesting anomaly by high field X-ray diffraction.

5. Summary

Through the combined efforts of materials discovery and specialized high-field laboratories worldwide, a steady progress of novel materials displaying exotic phases and phase transitions at high magnetic fields are emerging. Typical material classes are superconductors, multiferroics, magnetoelectrics and quantum magnets. In all such cases, a significant step towards a full understanding the microscopic physical processes responsible for the occurrence of these phases is the identification of magnetic, electric order parameters and of the lattice symmetry. The present project established the usefulness of pulsed magnetic fields for scattering experiments.

Reference

[1] T. Yamazaki *et al.*, Nucl. Instrum. Methods Phys Res. A **833** (2016)122.
[2] W. Knafo Jan *et al.* Nat. Commun. **7** (2016) 13075.
[3] R. Toft-Petersen *et al.*, Phys. Rev. B **95**(2017) 064421.
[4] S. Gerber *et al.*, Science. **350**, 949 (2015).
[5] H. Jan *et al.* PNCS **113** 12849(2016).

Keywords: high magnetic fields, neutron and X-ray scatterings, superconductivity
Pascal Manuel(ISIS Spallation Neutron Facility) and Hiroyuki Nojiri (Magnetism Division, IMR)
E-mail: nojiri@imr.tohoku.ac.jp
http://www.hfpm.imr.tohoku.ac.jp/ index.html

Activity Report

Workshops

FY 2016 Workshops

No.	Chairperson	Title of Workshop	Place	Date
16WS1	T. Matsuoka	3rd Intensive Discussion on Crystal Growth of Nitride Semiconductors (IDGN-3)	IMR Lecture Hall	2017.1.16-18
16WS2	T. Goto	11th International Workshop on Biomaterials in Interface Science (Innovative Research for Biosis-Abiosis Intelligent Interface Summer Seminar 2016)	Graduate School of Dentistry Lecture Hall, Tohoku. Univ.	2016.8.30-31

3rd Intensive Discussions on Growth of Nitride Semiconductors

The international workshop "3rd Intensive Discussion on Growth of Nitride Semiconductors" was held at Auditorium of Institute for Materials Research in Katahira campus, Tohoku University on January 16-18, 2017. About 50 specialists in the field of nitride semiconductors participated in this workshop including foreign researchers. The leading researchers in the fields of electronic devices, the crystal growth, and the characterization for devices presented each current status, and discussed on technical issues each other.

The international workshop "3rd Intensive Discussion on Growth of Nitride Semiconductors (IDGN-3)" was held on January 16-18, 2017.

Staring from the vapor-phase growth of GaN by H. P. Marcus and J. J. Tietjen in 1969, the research on nitride semiconductors has progressed with a focus on GaN. Nitride LEDs and LDs have been widely used as solid state lighting for energy saving and high-density recording such as Blu-ray, since blue LEDs became commercially available in 1996. Nitride transistors with high-frequency and high-power will come to realization in near future. Recently, nitride solar cells have been studied for covering over the whole range of solar spectrum. Thus, the device application has progressed in a variety of fields [1]; however, the crystalline quality is still poor in comparison with conventional III-V semiconductors such as GaAs and InP. For the future development in high efficiency, long device-lifetime, and the expansion of application, it is indispensable to improve the crystalline quality and to control the crystal characteristics.

The previous workshops (IDGN-1 and 2) held in 2012 and 2014 provided us the opportunity to share the most recent achievements and to discuss the technical issues on the crystal growth and device applications of nitrides. The purpose of the present workshop was to analyze the status quo, and to find the direction to take in the future and the problems that need to be solved in the field of high power and high breakdown voltage transistors, high frequency transistors, the epitaxial growth and the process technology for transistors. To achieve these, the number of participants was limited to 50 persons including researchers from abroad, and the straightforward discussion was greatly encouraged among the selected professionals. Participants had common understandings in the current technologies and found out the way to solve problems in the crystal growth. In the workshop, some selected topics were presented at the beginning of each session, and the participants voluntarily presented their data, which were followed by deep-and-intensive discussion. This style is not common but brought us the significant outcome.

The workshop chairs found a great deal of satisfaction in all the topics, and would like to say thank all the panelists and participants who boosted the fruitful discussion.

This workshop was supported by International Collaboration Center, Institute for Materials Research (ICC-IMR), Institute for Materials Research (IMR), and Institute of Multidisciplinary Research for Advanced Materials (IMRAM), Tohoku University.

References

[1] Selected Topics in Applied Physics "Progress of Nitride Semiconductors and their Future Prospects", ed. T. Matsuoka *et al.*, Jpn. J. Appl. Phys., vol. 53, No. 10, Oct. 2014.

Fig. 1 Participants selected professionals.

Keywords: nitride, crystal growth, epitaxy
Takashi Matsuoka (Physics of Electronic Material, IMR)
E-mail: matsuoka@imr.tohoku.ac.jp
http://www.matsuoka-lab.imr.tohoku.ac.jp/

The 11th International Workshop on Biomaterials in Interface Science

- Innovative Research for Biosis-Abiosis Intelligent Interface Summer Seminar 2016 -

Biosis-abiosis intelligent interface science has been developed as a concept to explore materials and systems between human constituents and biomaterials. Forefront researchers and students from various fields related to biomaterials gathered at the The 11th International Workshop on Biomaterials in Interface Science on Aug. 30–31st at Sendai, Japan. The Invited lectures by seven experts and nineteen contributed papers provided valuable opportunity for cross-over discussion, interdisciplinary idea sharing and new collaboration to develop and establish the intelligent interface science on biomaterials.

To develop biomaterials that can adopt in human bodies in a short time and be used over a long term, highly functional and autonomic intelligent interface is necessary to be created by combining the various topics of biomaterials, the technology of an evaluation and a control of the interface, innovation for oral science and application, regenerative oral science, and medical engineering [1]. Therefore, interdisciplinary and international research activities are necessary to understand complex phenomena occurring at the biosis-abiosis interface and to develop and biomaterials, such as artificial bone and tooth, optimizing the material design and systems. Three Institute in Tohoku University, namely Institute for Materials Research (IMR), Graduate School of Dentistry and Graduate School of Biomedical Engineering, have been collaborating and involved in the 5-year project on Biomaterials to establish a new concept, Biosis-Abiosis Intelligent Interface Science. As the series of international forums in the frame this project, the 11th International Workshop on Biomaterials in Interface Science in conjunction with Innovative Research for Biosis-Abiosis Intelligent Interface Summer Seminar 2016 was held by a new collaborative project “Creation of Life Innovation Materials for Interdisciplinary and International Researcher Development” on Aug. 30th–31st, 2016, at Tohoku University in Sendai.

The 2-days technical program in this workshop included 26 papers in which 7 invited lectures were given by distinguished professors and experts on biomaterials from Taiwan, China, Russia and Japan. 64 participants of professors, researchers and students attended in the workshop. Prof. Ming-Lun HSU who is the dean of School of Dentistry, National Yang-Ming University provided an invited lecture on prei-implant bone biomechanics. The invited lecture by Prof. Lenan SHAO was on lymphatic network and cancer metastasis. Prof. Kensuke KURODA gave a lecture on osteoconductivity and protein adsorbability of hydrophilic and hydrophobic titanium implants surface using hydroprocessing. The state-of-the-art research on odontogenic keratocyst was provided by Prof. Tie-Jun LI. Prof. Youfa WANG gave an invited lecture on PRGD/PDLLA/n-HAP composites for peripheral nerve regeneration. From the side of material science, two professors, Prof. Wei ZHANG and Prof Yu ZADOROZHNYY, introduce their updated research on metallic glasses and Ti-based materials. Contributed papers by speakers from a various fields, such as dentistry, bioengineering and biomaterials, provided their updated research. These invited lectures and oral presentations gave the all participants a valuable opportunity for sharing interdisciplinary viewpoints and ideas. These collaborative discussion had great contributions to the development on the intelligent interface science on biomaterials.

Fig.1 Group photo and shots in lectures.

References

[1] K. Sasaki, O. Suzuki, N. Takahashi Ed., Interface Oral Health Science 2016, (2016).

Keywords: Biomedical, ceramic, metal
Takashi GOTO (Multi-Functional Materials Science)
E-mail: goto@imr.tohoku.ac.jp
http://interface2016.imr.tohoku.ac.jp/

Activity Report

KINKEN WAKATE

FY 2016 KINKEN WAKATE

No.	Chairperson	Title of Workshop	Place	Date
16Wakate	H. Miyasaka	Workshop for Young Investigators on Functional Molecular Materials and Molecular Related Magnetism (KINKEN WAKATE 2016)	IMR Lecture Hall	2016.9.3-9.4

KINKEN WAKATE 2016: 13th Materials Science School for Young Scientists, "Workshop for Young Investigators on Functional Molecular Magnetism and Molecular Related Magnetism"

KINKEN WAKATE 2016, 13th Materials Science School for Young Scientists was held on 3rd-4th September, 2016 at IMR, which focused on a subject of molecular magnetism and molecular related functionalities and materials. In the workshop, three world researchers in the field of molecular magnetism and seventeen members of young investigators were invited as tutorial lectures and oral presenters, respectively, as well as poster presenters more than fifty members.

The titled workshop, 13th Materials Science School for Young Scientists (KINKEN WAKATE 2016): Workshop for Young Investigators on Functional Molecular Materials and Molecular Related Magnetism – Rising Star Pre-ICMM@IMR –, was held in the term of 3rd – 4th September, 2016 at the lecture hall in IMR. In the workshop, three world researchers in the field of molecular magnetism, Prof. Joel S. Miller, University of Utah, USA, Prof. Rodolphe Clérac, Centre de Recherche Paul Pascal, France, and Prof. Michel Verdaguer, Université Pierre et Marie Curie, France, were invited as tutorial lecturers. Prof. Miller, who is one of the leaders from an early stage of the development of molecular magnetism, presented own historical work on molecule-based magnets with organic radicals of TCNQ and TCNE. His wonderful examples on organic high T_c magnets and his strategy for the molecular design attracted us.

Prof. Clérac, who is one of the leaders in young researchers on molecular magnetism, presented works on magnetic materials associated with electron transfers. He talked about various types of multiple transitions such as spin-crossover with electron transfers and photo-induced spin-crossover. The control of multiple transitions in molecular systems is one of the most attractive themes in the field of molecular science.

Prof. Verdaguer, who is a leader of Prussian blue-type magnets, presented basic science on magnetic properties, in addition to a topic on his own historical works on Prussina blue-type high T_c magnets. He actually demonstrated some experiments at the lecture hall in IMR(!) to answer the following questions: *is oxygen really paramagnetic?* and *does the molecular magnet really be a magnet below T_c?* Everybody excited his lecture with demonstrations.

In addition to the tutorial lecture, seventeen members of young investigators had oral presentations, and more than fifty members had poster presentations on the first day evening.

In this meeting, we had a lively discussion not only on molecular magnetism, but also on much wider subjects of materials science. Finally, we had total 112 members of participants (65 from oversees + 47 from domestic areas), who joined from 14 countries (USA, France, Australia, Spain, Poland, Canada, Germany, UK, China, Russia, Swiss, Slovakia, Ukraine, and Japan).

On behalf of the organizing committee, I acknowledge the organizer members and Miyasaka group members for help on the management of the symposium, as well as all participants in the symposium.

Keywords: magnetic properties
Hitoshi Miyasaka (Solid-State Metal-Complex Chemistry)
E-mail: miyasaka@imr.tohoku.ac.jp
http://www.miyasaka-lab.imr.ac.jp/ index.html

Activity Report

Short-term Visiting Researchers

FY 2016 Short-term Visiting Researchers

Application No.	Name	Host	Proposed Research	Title	Affiliation	Term
16SV1	Lech Tomasz Baczewski	K. Takanashi and M. Mizuguchi	Structural and Magnetic Studies of the L10 FeNi Ordered Alloys with High Magnetic Anisotropy	Professor	Institute of Physics Polish Academy of Sciences, Poland	2016.5.11-5.28
16SV2	Albert Chi Fu To	Y. Koizumi	Optimization of Variable-Density Cellular Structured Metal Component	Associate Professor	University of Pittsburgh, USA	2016.9.11-9.26
16SV3	Mariya Zhuravleva	A. Yoshikawa	Eu Dopant Segregation in Ternary Scintillator Crystals Grown by the m-PD and Bridgman Methods	Assistant Professor	University of Tennessee, USA	2016.12.5-12.22
16SV4	Andery Medvedev	A. Yoshikawa	Development of Novel Oscillator Using Langasite-Type Piezoelectric Single Crystal	Technical Director	Fomos-Materials Corporation, Russia	2016.2.1-3.1
16SV5	Takuya Yamamoto	K. Nagai	Effects of Mn Content on the Characteristics of Radiation Induced Defects in Reactor Pressure Vessel Steels	Professional Researcher	University of California Santa Barbara, USA	2016.11.11-30
16SV6	Anucha Watcharapasorn	T. Goto	Investigation of Potential Thermoelectric Oxides Prepared by Spark Plasma Sintering	Assistant Professor	Chiang Mai University, Thailand	2016.10.1-10.16
16SV7	Mikhail Titov	G. Bauer	Spin-Transfer Torques in Ferromagnetic and Antiferromagnetic Systems with Spin-Orbit Interaction	Assistant Professor	Radboud University Nijmegen, the Netherlands	2017.1.9-24
16SV8	Junichiro Kono	H. Nojiri	Terahertz Time-Domain Spectroscopy in Pulsed Magnetic Fields up to 30 Tesla	Professor	Rice University, USA	2017.2.6-2.15 Gary Timothy Noe II Fumiya Katsutani

Structural and Magnetic Studies of the L10 FeNi Ordered Alloys with High Magnetic Anisotropy

Iron based thin films systems were studied: FeNi and FePt. Both systems are interesting in view of possible practical applications in perpendicular magnetic recording. FeNi thin films were grown by sputtering method in IMR on MgO(100) monocrystalline substrate and Fe/Pt multilayers were prepared by MBE on sapphire substrates in IPPAS in Warsaw. In both systems studied the aim is to obtain the ordered phase L10 with high perpendicular anisotropy.

The aim of the study within the scientific collaboration between IMR and IPPAS is to obtain metallic magnetic thin films with high perpendicular magnetic anisotropy for application in magnetic recording. Two iron based thin films systems were studied: FeNi and FePt. I was collaborating with prof. M. Mizuguchi on FeNi and with prof. T. Seki on Fe/Pt system in the prof. K. Takanashi Magnetic Materials Laboratory at IMR.

FeNi thin films were grown by sputtering method at IMR on MgO(100) monocrystalline substrate and Fe/Pt multilayers were prepared by MBE on sapphire (0001) substrates at IPPAS in Warsaw. Sputtered FeNi thin films were deposited directly on MgO substrate without any buffer layer to avoid any interdiffusion during post growth annealing at 300 C by RTA method and in order to have a simple, not costly as MBE and easy method of growing of L10 FeNi phase. The long-range chemical order parameter (S) was precisely estimated by grazing incidence X-ray diffraction (GI-XRD) using synchrotron radiation at SPring-8 in the Japan Synchrotron Radiation Research Institute. S parameter was estimated from the intensity ratio between a superlattice (110) peak and fundamental (220) peak seen on the diffraction pattern. However the highest value of S of about 0.3 was obtained what is significantly lower than for MBE grown films on a relevant buffer layers[1,2]. Another type of substrates such as spinel and SrTiO3 with smaller misfit values were tried but with no success – lower S values were found or no superlattice (110) peaks were observed. For now the reason for such behavior is not clear. In the next stage of the study based on theoretical predictions, the addition of 2-5 % of Ti and V replacing Ni in the multilayered structure was tried. Vanadium addition did not help at all the formation of L10 FePt alloy phase and Ti addition helped but only in a limited way. It seems there is a major drawback in obtaining pure ordered L10 phase of FeNi alloys. Also surfactants of O and Au were tried [3]- the largest Ku were 0.58 MJ/m3 for O-surfactant and 0.42 MJ/m3 for Au-surfactant. It has been concluded that the reason for the appearance of large Ku by using surfactants is attributed to the enhancement of the L10-ordering of FeNi. However it is still far from the value of 1.3 MJ/m3 reported for bulk FeNi single crystals. FMR measurements revealed peculiar in plane symmetry – two-fold, four-fold and even six- fold depending on the preparation method. However further detailed resonance field signal analysis including asymmetry of resonance lines and their widths revealed that peculiar six or eight fold

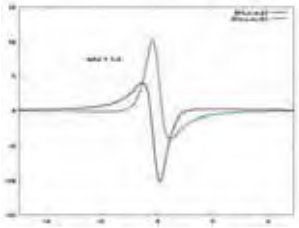

Fig.1 FMR resonance line shape for asymmetry parameter beta = 0 (green line) and 2 (violet line).

symmetry observed for MBE grown samples disappeared and was transformed into classic two-fold one typical for cubic structure. In Fig.1 one can see the exemplary shape of resonance line for asymmetry parameter beta equal 0 (symmetrical line) and 2 (asymmetrical line).

Taking into account the asymmetry of observed resonance lines we were able to explain peculiar shape of the angular in-plane dependence of the resonance field measured by ferromagnetic resonance (FMR). Below one can see how this angular dependence changes when the asymmetry is taken into account.

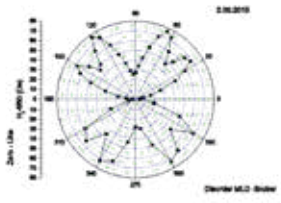

Fig. 2 Angular in-plane dependence of the FMR resonance field for asymmetry parameter beta= 0 – MBE grown sample, not annealed.

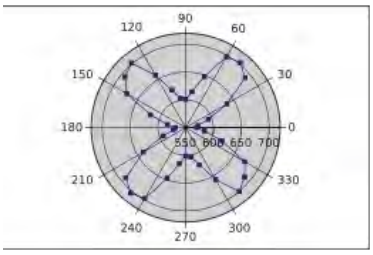

Fig.3 Angular in-plane dependence of the FMR resonance field for asymmetry parameter beta= 1 for the same MBE sample, not annealed.

Comparing Figs. 2 and 3 one can easily see that strange symmetry in Fig. 2 was changed into two-fold symmetry typical for cubic structure and expected for L10 structure of FeNi alloy.

Summarizing we have tried to grow FeNi alloys as thin films structure on different substrates and buffers, changing growth conditions and deposition methods but we have not succeeded to obtain high ordered samples in pure L10 structure. However the preparation of a publication of the obtained results is in progress.

Concerning the magnetic anisotropy modification by ion irradiation in Fe/Pt thin films the results were published in a common publication:

Structural and magnetic properties of MBE grown (Fe/Pt) (111) multilayers

A Marynowska, E Dynowska, S Lewińska, T Seki, K Takanashi, J Kanak, A Pietruczik, A Wawro, A Ślawska-Waniewska and L T Baczewski

Acta Physica Polonica A.,vol. 130 (6) p. 1363 (2016)

References

[1T. Kojima et al. Jpn J Applied Physics 51 (2012) 010204

[2] T. Kojima et al. J. Phys. Cond Matter.26 (2014)

[3] T. Kojima, M. Mizuguchi, T. Takanashi, Thin Solid Films, 603, (2016) 348

Keywords: magnetic properties, metallic thin films,

Full Name: prof. Lech T. Baczewski, Department of Magnetism, Institute of Physics, Polish Academy of Sciences, Warsaw, Poland
E-mail: bacze@ifpan.edu.pl
http://www.ifpan.edu.pl

Finite element analysis of Elastic Property of Biomedical Co-Cr-Mo Lattice Structure Fabricated by Electron Beam Powder Bed Fusion

Our objective is to apply finite element analysis to compute equivalent modulus of cellular lattices of biomedical Co-Cr-Mo-alloy with optimization shape. Firstly, the finite element analysis (FEA) model is established to predict effective elastic tensor of a 4×4×4 cells based on experimental boundary conditions. Effective elastic tensor predicted by FEA simulation is compared with experimental results. For ρ =0.3, the results of elastic tensor prediction show that computational model achieves good agreement with experimental data to some extent. However, for ρ =0.2, there exists some difference between experimental data and computational model in x direction.

With a view to developing a biocompatible and reliable material to be embedded in femoral bone, cellular lattice structures with high strengths and low Young's moduli (E) are highly desired. Additive manufacturing (AM) of cellular lattices are promising candidates owing to the tunability of mechanical properties. We applied finite element analysis based on Dirichlet boundary conditions to obtain the effective elastic properties of cellular lattices of biomedical Co-Cr-Mo-alloy with optimized shape for different relative densities (ρ). Boundary condition $u_z = 0$ mm is applied at the bottom surface and $u_z = -1$ mm is applied at the top surface. To eliminate rigid body displacement, two points at bottom are fixed. Triangular mesh is generated in this case with 2,997,440 elements. The material properties employed in the FEA are shown in Table 1.

The distribution of total von-Mises stress evaluated by FEA for ρ=0.2 is shown in Fig. 1. In this case, we apply

$$\varepsilon_z = 1,\ \varepsilon_x = \varepsilon_y = \gamma_{yz} = \gamma_{xz} = \gamma_{xy} = 0 \qquad (2)$$

The strain energy S is

$$S = \frac{1}{2} E_z \varepsilon_z^2 \cdot V \qquad (3)$$

where V is volume of cells. According to Eq. (3), the equivalent modulus of cells in z direction is derived from the strain energy obtained thru FEA, and the resulting value is shown in Table 2. Similarly, equivalent elastic modulus in x direction is obtained and resulting value is given in Table 2. The equivalent modulus in the z direction obtained for from FEA can agree with experimental result to some extent, with error around 16.4%. However, in x direction, there exists a relatively large difference between experimental and numerical results, with error around 39%.

Table 1. Material properties used for FEA

E_Z (GPa)	E_X, E_y (GPa)	G_{xz}, G_{zy} (GPa)	ν_{xy} (–)
150	200	50	0.15

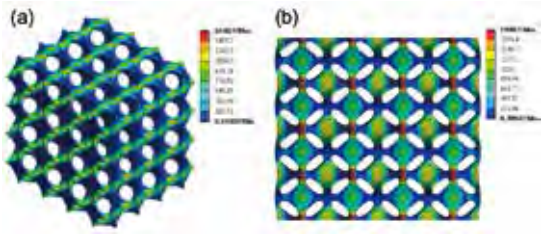

Fig. 1 Finite element result from compression in z-direction showing (a) bird's eye view, (b) von Mises stress, and (c) strain energy.

For ρ=0.3, similar procedure is conducted using FEA, and the equivalent moduli obtained can be found in Table 3. It is obvious that elastic modulus E_z from FEA achieves great agreement with experimental data, with error less than 5%. For elastic modulus E_x, experimental result is higher than FEM results, with error less than 15%.

Table 2. Equivalent modulus for ρ=0.2

	Experiment (GPa)	Numerical (GPa)	Error (%)
E_z	11.2	9.36	-16.4
E_x	20	12.09	-39.5

Table 3. Equivalent modulus for ρ=0.3

	Experiment (GPa)	Numerical (GPa)	Error (%)
E_z	17.6	18.03	2.4
E_x	26.8	23.24	-13.28

References

[1] M. Long, H.J. Rack. Biomaterials 19 (1998) 1621-1639
[2] J. Yan, G. Cheng, S.Liu, L. Liu, Int. J. Mech. Sci. 48 (2006) 400–413
[3] Y. Koizumi et al. Add. Man. 12 (2016) 305-313.

Keywords: biomedical, cellular (material form), mechanical properties
TO, Albert Chi Fu (Department of Mechanical Engineering and Materials Science, University of Pittsburgh)
E-mail: albertto@pitt.edu
http://www.pitt.edu/~albertto/

Crystal growth of $KCaI_3$:Eu and KSr_2I_5:Eu scintillators using the micro-pulling-down method

We demonstrated crystal growth of inorganic ternary scintillators $KCaI_3$:Eu and KSr_2I_5:Eu using a unique micro-pulling-down method that was developed for highly hygroscopic halides. These novel materials are very promising for use in gamma-ray spectroscopic detector applications related to nuclear nonproliferation and domestic security due to their superior energy resolution and scintillation light output. Fast pulling rates offered by this growth method also allow to study and improve axial segregation of the Eu luminescent activators.

We conducted crystal growth experiments using the micro-pulling-down (m-PD) method at Tohoku University. We explored experimental parameters such as the thermal gradient of the hot zone, pulling-rates (0.03 -0.09 mm/min), geometry of the crucibles and after-heaters, and melt history. We also compared two different forms of raw materials: pre-synthesized ternary compounds vs stoichiometric mixtures of binary halides. Raw materials were anhydrous, 4N-5N pure binary halides and were obtained commercially.

As a result, we successfully developed reliable growth protocols. Figure 1 shows grown single crystals of $KCaI_3$:Eu and KSr_2I_5:Eu scintillators. The crystals were 3 mm dia. and 15-20 mm long cylinders with high translucency and adequate shape control. We determined that fine powders are not suitable for pre-synthesis, and that larger chunks of pre-synthesized material must be used instead. We found that vibrations in the pulling mechanism caused unstable growth conditions and prevented from using pull rates above 0.09 mm/min. Additionally, due to high hygroscopicity of the crystals, it was challenging to handle sample preparation for characterization.

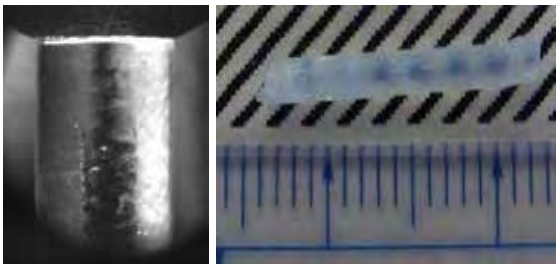

Fig. 1 *In-situ* view of stable growth conditions during the micro-pulling-down experiment and the resulting crystal of $KCaI_3$:Eu.

crystals in our laboratory at the University of Tennessee, USA. Photo- and radioluminescence as well as luminescence kinetics were measured. Figure 2 shows an important characteristic for gamma-ray spectroscopy applications, I.e. the energy resolution at ^{137}Cs (662 keV). Based on the energy resolution, light output and scintillation non-proportionality, both $KCaI_3$:Eu and KSr_2I_5:Eu are highly competitive with novel commercial scintillators such as SrI_2:Eu and $LaBr_3$:Ce. Good scintillation non-proportionality and energy resolution are also indicative of high crystalline quality obtained via the m-PD method.

The research results of this work will be presented at the American Crystal Growth

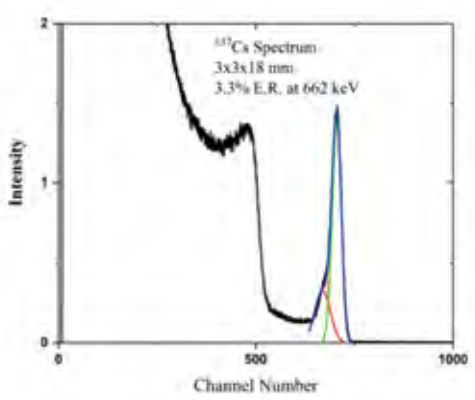

Fig. 2 Gamma-ray spectrum of $KCaI_3$:Eu showing energy resolution of 3.8% at 662 keV and ~70,000 ph/MeV light output.

Conference, July 30 – August 4, Santa Fe, NM, USA. The abstract entitled "Crystal growth of $KCaI_3$:Eu and KSr_2I_5:Eu scintillators using the micro-pulling-down method" has been accepted for a poster presentation.

Keywords: crystal growth, radiation effects, luminescence
Mariya Zhuravleva (University of Tennessee, Scintillation Materials Research Center)
E-mail: mzhuravl@utk.edu
http://www.engr.utk.edu/smrc/

Novel Oscillator Using Langasite-Type Piezoelectric Single Crystal

Appropriate configuration of novel resonator using langasite-type piezoelectric single crystal was designed. The resonator is able to achieve lower impedance at low frequency range, faster start up time, and wider band performance as compared with conventional quartz resonator and to contribute to downsizing and low power consumption of on-board equipment.

Langasite-type single crystals are attractive materials for high-stability oscillators and filters as well as pressure sensors operating in high-temperature environments. Novel langasite-type single crystal was developed from a compound reducing scarce elements as compared to conventional one (Fig. 1) [1]. When applying the novel langasite-type single crystal to a resonator, it contributes to low power consumption of the instrument on board because of the properties such as low impedance at low frequency and fast start up time which are unachievable with quartz.

Fig.1 Novel langasite-type single crystal.

All electronic devices operate based on the reference signal called “clock signal”. The resonator is one of the key devices generating the clock signal. Because the clock signal is generated based on the signal at the resonant frequency of the resonator, it is important to design the resonator without spurious signals around the resonant frequency for stable generation of the clock signal. The spurious appears depending on cut angle of the crystal, operating frequency, configuration of the crystal substrate (length, width, and thickness), shape of electrode, and so on.

In this report, appropriate configuration of the resonator without spurious around resonant frequency 8 MHz was investigated taking a rotated Y-cut substrate as specimen.

In theoretical consideration of the spurious, Mindlin’s plane plate equation [2] and material constants determined were applied in the calculation. Resonator thickness h=0.185 mm and frequency constant C=1507 were used as calculation parameters for designing resonant frequency of 8 MHz. The result was shown in Fig. 2. The lateral axis is l_x/h, where l_x and h are length and thickness of resonator. The vertical axis is ω/ω_0, where ω is frequency and ω_0 is resonant frequency of infinite plate.

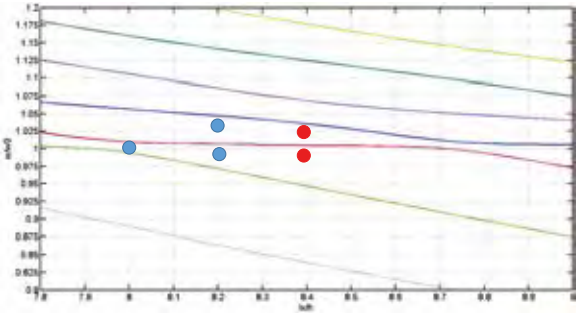

Fig. 2 Mode chart of resonator.

In Fig. 2, solid lines are the calculated results and dots indicate the results of main resonant and neighbor spurious components obtained from the experimental measurement. Difference between the calculated and measured results are considered to be the mass-loading effect of electrode. From the above results, l_x/h=8.3 is expected to be appropriate configuration for the resonator because there are no spurious components near the main resonance.

References

[1] A. Yoshikawa, Y. Shoji, Y. Ohashi, Y. Yokota, V.I. Chani, M. Kitahara, T. Kudo, K. Kamada, S. Kurosawa, A. Medvedev, V. Kochurikhin, ”Czochralski growth of 2 in. $Ca_3Ta(Ga,Al)_3Si_2O_{14}$ single crystals for piezoelectric application”, J. Cryst. Growth, 452, 135 (2016).

[2] Raymond D. Mindlin, “Compliance of elastic bodies in contact”, J. Appl. Mech. 16, 259 (1949).

Keywords: crystal, piezoelectric, devices
Full Name: Andrey Medvedev (Fomos Materials)
E-mail: medvedev@imr.tohoku.ac.jp
http://www.newpiezo.com

Effects of Mn content on the characteristics of radiation induced defects in reactor pressure vessel (RPV) steels

Mn effects on the formation of displacement cascade-induced defects, cascade fragments (CF), in RPV steels, which can be enhanced in accelerated irradiations at high dose rates, was examined using high flux test reactor as well as Fe^{2+} ion irradiation. No hardening was observed in the alloy containing 0% Mn, while the hardening increases with Mn to reach commonly observed level of CF hardening in ion irradiation at Mn ≥ 1.4%, suggesting low Mn can suppress the CF formation.

The current prediction model of irradiation hardening and embrittlement of RPV steels under-predicts brittle to ductile transition temperature shift (TTS) of steels irradiated in test reactors to high neutron fluence (ϕt) [1] partially due to cascade fragments (CF) formed in displacement cascades. The CFs continuously anneal during reactor operation, but build up at high flux (ϕ) in test reactors, causing additional hardening. At the same time, higher flux accelerates point defects recombination to reduce the radiation enhanced solute diffusion, that delays formation of other types of hardening features. Thus in high flux test reactor, hardening and embrittlement trends are different from power reactor conditions. Never the less, utilizing test reactor data is necessary in order to predict long-term (high dose) TTS trends. Thus, the purpose of the research is to understand CF characteristics and the behavior, which will be used to develop a method that properly accounts for the effects of high flux and CF formation in evaluating test reactor irradiated specimens.

RPV model steels of chemistry variation including Mn varied from 0 to 1.6 % are irradiated in a Belgium test reactor, BR2, followed by micro Vickers hardness tests, which is complemented by nano-hardness measurements carried out on a subset of alloys irradiated by 2.8 MeV Fe^{2+} ion in HIT facility in University of Tokyo.

Figure 1 shows hardness change, ΔHv, as a function of neutron fluence for steelss with various Cu-Ni-Mn compositions. ΔHv is higher for 0.4% Cu steels and showed steeper increase at the highest dpa in high Ni alloys presumably due to Mn-Ni-Si precipitates (MNSP) formation. The trends are very consistent with our previous results on the steelss. Medium 0.8% Mn trend is similar to 1.4% Mn, while 0% Mn alloy showed ΔHv ≈ 0. Figure 2 shows nano-hardness based ΔHv in ion irradiated 0% Cu-0.8% Ni steels with 0 to 1.6% Mn. The figure also show CF hardening trend previously observed commonly in 0 to 0.2%Cu-1.4%Mn-0.8%Ni alloys. The 1.4-1.6%Mn data follow the common CF trend within the scatter, 0.8%Mn falls slightly lower, but 0%Mn shows much lower almost no hardening. Figure 3 summarizes the Mn dependence of hardening in these two series of irradiations. Here neutron dose is converted to corresponding dpa using dpa cross section of 1.5×10^{-21} cm^2. The most distinctively the ΔHv is ≈ 0 for 0% Mn, which generally increase with Mn except low dose conditions including ion 0.01 and BR1 0.04 dpa. In these cases, hardening is ≈ 0 for all Mn level. Since the hardening in ion irradiation is mostly due to the CF, low Mn seems to suppress CF formation at least in ion irradiation. For BR2 neutron irradiation, post irradiation annealing study will be carried out to isolate the CF hardening component from the total.

References

[1] G.R.Odette and R.K.Nanstad, JOM 61 (2009) 17

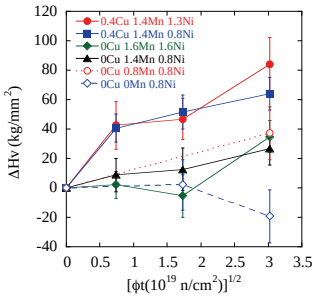

Figure 1 Neutron dose dependence of hardness change in RPV steels with 0-0.4Cu, 0-1.6Mn and 0.8-1.3Ni in BR2 test reactor.

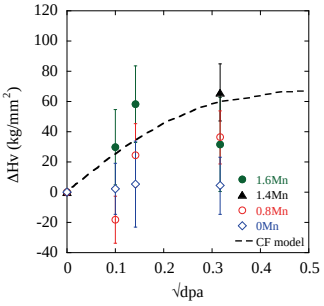

Figure 2 dpa dependence of hardness change in RPV steels containing 0%Cu, 0.8%Ni and various (0 to 1.6%) Mn irradiated by Fe2+ ion.

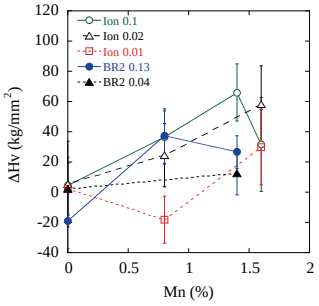

Figure 3 Mn dependence of hardness change in 0Cu-0.8Ni RPV steels to various doses in BR2 reactor or in Fe^{2+} irradiation.

Keywords: nuclear materials, radiation effects, positron annihilation

Takuya Yamamoto (Univ. California Santa Barbara)
Collaborators: Peter Wells, G. Robert Odette (UCSB), Takeshi Toyama, Yasuyoshi Nagai (Tohoku U.), Kenta Murakami (U. Tokyo) and Hideo Watanabe (Kyushu U.)
E-mail: yamataku@engineering.ucsb.edu

Thermoelectric properties of $Ca_3Co_4O_9$-$Bi_{0.5}Na_{0.5}TiO_3$ and Na_xCoO_2-$Bi_{0.5}Na_{0.5}TiO_3$ ceramics fabricated by spark plasma sintering

P-type layered cobalt oxides, Na_xCoO_2 (NCO) and $Ca_3Co_4O_9$ (CCO), are currently the two most investigated compounds with highest thermoelectric conversion performance for high-temperature energy harvesting applications[1,2,3]. Above 700 K, the ZT values for NCO and CCO can reach the value of about 0.8 – 1.0[3,4]. However, it is practical to investigate these compounds in order to improve their performances at lower temperature range for the purpose of replacing the current non-oxide compounds used in thermoelectric devices. The advantages of these compounds include the ease of fabrication and stability against oxidation environment. By employing cationic and anionic substitution using $Bi_{0.5}Na_{0.5}TiO_3$ (BNT), we hope to obtain a systematic favorable change in thermoelectric properties of these compounds.

In this study, a varying amount up to 0.07 mol fraction of BNT powder was doped in CCO and NCO powders by mechanical mixing in ethanol. Ceramics were fabricated by spark plasma sintering (SPS) the CCO-*x*BNT and NCO-*x*BNT mixtures at 900 °C (5 min) and 850 °C (3 min), respectively, under the pressure of 100 MPa in vacuum.

For CCO-*x*BNT ceramics, it was found that small addition of up to 0.03BNT caused a decrease in electrical conductivity while the Seebeck coefficient increased. With higher doping concentration, the opposite effects occurred. Since the thermal conductivity was lower only when 0.01BNT was added to CCO, the maximum value of ZT was obtained for CCO-0.01BNT ceramic as shown in Fig. 1. Due to the increasing trend of Seebeck coefficient with increasing temperature, this resulted in the larger ZT values at higher temperature. Overall, the thermoelectric performance of CCO-xBNT ceramics was virtually independent of BNT concentration.

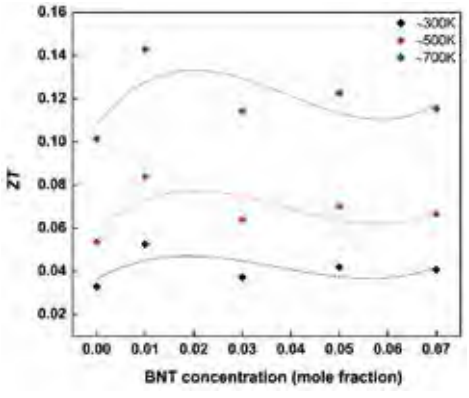

Fig. 1. The variation of ZT values of CCO-xBNT ceramics with BNT content at various temperatures.

Keywords: ceramic, oxide, thermoelectric
Full Name: Anucha Watcharapasorn, Department of Physics and Materials Science, Chiang Mai University, Thailand
E-mail: anucha@stanfordalumni.org

The ZT values for NCO-xBNT ceramics are shown in Fig. 2. In contrast to the CCO-xBNT system, the addition of BNT caused the thermoelectric performance to decrease. This was mainly due to a large reduction of the electrical conductivity by nearly one order of magnitude while Seebeck coefficient remained about the same values regardless of added BNT content. The thermal conductivity was reduced only at small doping concentration.

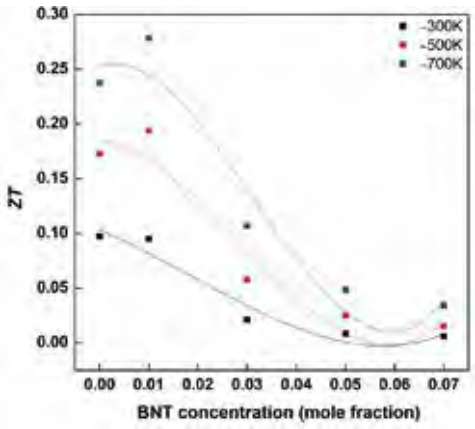

Fig. 2. The variation of ZT values of NCO-xBNT ceramics with BNT content at various temperatures.

From this investigation, a small BNT addition (≤ 0.03 mol fraction) could result in a slight increase in thermoelectric performance in both CCO and NCO compounds while no advantage was gained with addition of higher BNT content.

References

[1] I. Terasaki, Physica., 2003, B328:63-67.
[2] P.H. Xiang, Y. Kinemuchi, H. Kaga, K. Watari, J. Alloy. Compd., 2008, 454:364-369.
[3] N. Li, Y. Jing, G. Li, C. Wang, J. Shi, D. Yu, J. Alloy. Compd., 2009, 467:444-449.
[4] D. Wang, L. Cheng, Q. Yao, J. Li, Solid. State. Commun., 2004, 129:615-618.

Spin-Transfer Torques in Ferromagnetic and Antiferromagnetic Systems with Spin-Orbit Interaction

We formulated a general microscopic approach to spin-orbit torques in thin ferromagnet/heavy-metal and antiferromagnet/heavy-metal bilayers in linear response to electric current or electric field. The microscopic theory we develop avoids the notion of spin currents and spin-Hall effect. Instead, the torques are directly related to a local spin polarization of conduction electrons, which is computed from generalized Kubo-Streda formulas.

The dynamic response of magnetization to electric currents flowing in the system is an interesting problem that has numerous applications. The rise of ferromagnetic, and recently antiferromagnetic, spintronics that promises controllable ferromagnetic or antiferromagnetic (AFM) domain switching with particularly low currents adds a number of challenges in the field. At the same time, the ferromagnetic (FM) layers on the top of heavy-metal materials like Pt continue to be developed to become more sensitive to in-plane electric currents, see Fig. 1. Phenomenological approaches to spin torques, which have been proposed so far, ignore the role of spin-orbit interaction. An additional complexity arising in antiferromagnetic systems makes phenomenological approach even less useful since the underlying system symmetry is so complex that the number of free phenomenological parameters in such theories tends to infinity.

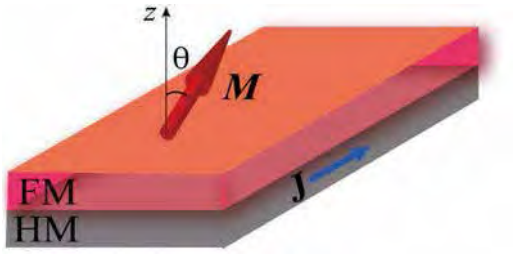

Fig. 1 Schematic of the studied system.

On the contrary, we use a microscopic approach, where we employ the framework of an *s-d* model, i.e. we separate a subsystem of localized spins (“d-electrons”) in the FM or AFM system from the subsystem of itinerant (conduction) electrons (or “s-electrons”). The magnetization dynamics of the FM subsystem is then investigated on the basis of the local mean field approach. The main idea of this approach f FM with localized spins is described by a classical magnetization field with constant length. The ground state of the FM is determined by the minimum of the free energy, which disregards the effects of itinerant electrons. The Landau-Lifshitz-Gilbert equation for the magnetization dynamics in this approach is governing this process.

We have shown that a unique dissipative-torque does not exist in a system with spin-orbit interaction. Instead, the lower symmetry of the model with Rashba interaction leads to the decomposition of the torques [1]. Moreover, the presence of spin-orbit interaction can increase the amplitude of dissipative spin-orbit torques by orders of magnitude. These and other consequences of the simple symmetry analysis based on microscopic models may have a predictive power that is absent as a matter of principle in a phenomenological approach to the problem. The results can be reproduced by a kinetic equations based on the Boltzmann-like equation for the lesser Green function. This allows us for the first time to consider the torques acting on magnetization independent of the angle between magnetization and two-dimensional plane of the heavy-metal layer.

In a follow-up we would like to extend the analysis to simple two-dimensional antiferromagnets (AFM) with spin-orbit interaction. The need for such a research is dictated by the fast development of AFM applications that involve current-induced AFM domain switching, e.g. the active development of the AFM MRAM devices that utilize heavy-metal/AFM bilayers. Our analysis will serve as an important benchmark to test kinetic equation methods and various numerical approaches to the problem that will be developed to treat realistic AFM devices.

References

[1] I. A. Ado, Oleg A. Tretiakov, and M. Titov, Phys. Rev. B **95**, 094401 (2017).

Keywords: spintronics, magnetic, texture
Mikhail Titov (Radboud University, Nijmegen, The Netherlands)
E-mail: m.titov@science.ru.nl
http://www.bauer-lab.imr.tohoku.ac.jp/

Title: Terahertz Time-Domain Spectroscopy in Pulsed Magnetic Fields up to 30 Tesla

Terahertz time-domain spectroscopy (THz-TDS) allows one to study low-energy dynamics in condensed matter systems such as traditional semiconductors, carbon nanotubes, heavy-fermion metals, Kondo insulators, high-temperature superconductors, and graphene by determining the complex conductivity. With applied magnetic field, various elementary and collective THz excitations occur associated with spin and orbital quantization.

This collaboration between IMR and Rice University has focused on ultrafast spectroscopy in pulsed high magnetic fields. We have developed a pulsed magnet system to measure the ultrafast and nonlinear response of materials in high magnetic fields up to 30 T and at low temperatures [1].

Recently at Rice University, we have developed a single-shot THz-TDS measurement system to measure the low-energy dynamics of materials with the pulsed magnet [2]. Our first measurements with this system were performed using intrinsic bulk silicon where we measured cyclotron resonance absorption to determine the effective mass of photoexcited carriers.

Currently, we have begun to study orthoferrite materials including $YFeO_3$ to determine how the ferromagnetic modes respond to applied high magnetic fields using the single-shot THz system. These materials hold promise for the manipulation of spins and understanding the fundamental interactions is crucial for development into viable technologies.

Figure 1 shows the THz time-domain waveform transmitted through $YFeO_3$ at 30 T and 0 T. By subtracting the two traces, one can isolate the frequency component that emerges at high magnetic field. The trace at 30 T is the average result after taking 25 measurements with a 7 minute wait time between magnet shot taking a total of ~3 hours. In order to also measure the magnetic field dependence in a reasonable amount of time, we must increase the efficiency of the data taking process. We have recently incorporated a high frame rate camera to take data during the entire ~10 ms duration of the magnet pulse instead of taking only one data point at the peak of the field.

Furthermore, we aim to increase the rate at which magnetic field pulses can be made. After each magnet shot, the coil must cool back to liquid nitrogen temperature after Joule heating. We have discussed changing the magnet pulse profile from an exponentially damped sine wave to simply a half sine wave where less total heat is created in the coil so that the cooling time decreases but still maintaining the same peak magnetic field strength. In the same amount of time, we could make more shots further increasing the the signal-to-noise ratios (SNRs) achievable with our system.

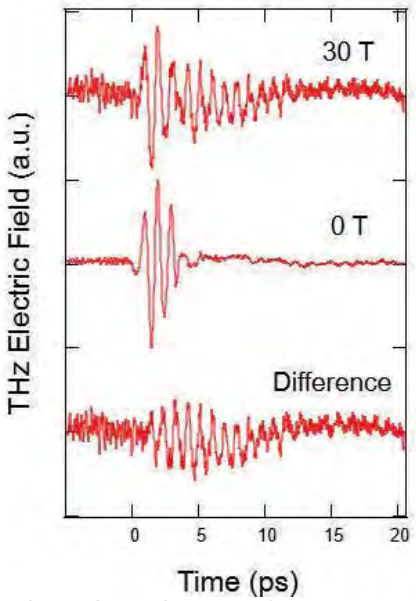

Fig.1 THz time-domain waveforms transmitted through orthoferrite $YFeO_3$ at 30 T and 0 T. The difference of the two traces reveals a new frequency component, ~1 THz, emerges at 30 T.

Furthermore, there is a future option to upgrade the control unit of our magnet system to automatically trigger the discharge of the capacitor bank for simple and easy operation so that we can automatically average over a large number of magnet shots.

At the IMR facility during our recent visit, Prof. Nojiri's group developed a smaller coil than our current 30 T coils located at Rice University. This new coil can achieve a magnetic field of 35 T, increasing the maximum field by over 16%. With a smaller coil, we lose the ability to insert a coldfinger

extension into the bore of the magnet to cool the sample however $YFeO_3$ does not have to be cooled to cryogenic temperatures in order to see the ferromagnetic resonance in the THz range. Therefore, this smaller coil is well suited for THz-TDS measurements of orthoferrite materials up to 35 T.

Fig.2 A new 35 T minicoil magnet developed at the IMR facility for THz-TDS measurements at Rice University.

In addition to orthoferrite materials, we are currently planning measurements of the THz response of graphene, aligned carbon nanotubes, high-temperature superconductors, and semiconductor quantum well samples.

References

[1] G. T. Noe et al., Rev. Sci. Instrum. **84**, 123906 (2013).
[2] G. T. Noe et al., Optics Express **24**, 30328 (2016).

Keywords: magnetooptic, high magnetic field
Full Name Dr. G. Timothy Noe II, Electrical and Computer Engineering Department, Rice University, Houston, Texas 77005
E-mail: TimNoe@rice.edu
http://www.kono.rice.edu

Activity Report

Young Researcher Fellowships

FY 2016 Young Researcher Fellowships

No.	Name	Host	Proposed Research	Title	Affiliation	Term
16FS1	Arina Ukhina	H. Kato	Development of Porous Graphitic Carbon Materials by Spark Plasma Sintering and Selective Dissolution Using Fe-Subgroup Metals as Graphitization Catalysts and Space Holders	PhD Student	Institute of Solid State Chemistry and Mechanochemistry, SB RAS, Russia	2016.7.2-8.15
16FS2	Arthur Seiji Nishikawa	T. Furuhara	Characterization of Products of Competitive during Quenching and Partitioning Applied to a Ductile Cast Iron	PhD Student	University of Sao Paulo, Brazil	2016.6.29-9.6
16FS3	Sougata Mallick	K. Takanashi	Geometrical Dependence of Magnetic Properties for Magnetic Antidot Lattices of Heusler Alloy	PhD. Student	National Institute of Science Education and Research, India	2016.10.30-12.25
16FS4	Hua Wang	E. Saitoh	Enhancement of Thermally Injected Spin Current in Epitaxial Pt/CoO/YIG	PhD. Student	Fudan University, China	2016.11.16-2017.1.15
16FS5	Jared Kinyon	H. Nojiri	Multiferrocity in the Gapless Quantum Antiferromagnet NH_4CuCl_3	Research Associate	Florida State University, USA	2017.1.5-3.31
16FS6	Guk No Yun	H. Kato	Developing Water-Etchable Melt for LMD (Liquid Metal Dealloying) Process	Ph.D. Candidate	Seoul National University, Korea	2016.12.21-2017.2.24

Development of Porous Graphitic Carbon Materials by Spark Plasma Sintering and Selective Dissolution Using Fe-Subgroup Metals as Graphitization Catalysts and Space Holders

In this work, carbon-based materials were obtained by graphitization-accompanied sintering of mixtures containing non-graphitic forms of carbon (nanodiamonds or amorphous carbon) and nickel, iron or cobalt as graphitization catalysts. The influence of the nature of the metal catalyst and the initial carbon source and the conditions of Spark Plasma Sintering and post-dissolution high-temperature annealing on the phase composition, structure, and properties of the porous carbon materials was investigated.

Porous graphitic materials with high graphitization degrees, high specific surface area, stable pore structure and mechanical robustness are attractive from the practical point of view as electrode materials for electrochemical devices. The purpose of this research was to evaluate the possibilities of producing porous graphitic carbon, including self-standing 3D objects, by conducting graphitization in the bulk state during Spark Plasma Sintering in the presence of Fe-subgroup metal catalysts, also playing a role of space holders, followed by selective dissolution of the metal, and gain an understanding of the influence of the processing variables (nature of the metal catalysts selected from Fe-subgroup metals and initial carbon source, Spark Plasma Sintering conditions, post-dissolution high-temperature annealing) on the phase composition, structure and properties of the porous carbon materials.

The graphitization degree of the amorphous carbon or nanodiamonds in the presence of nickel or cobalt increased with increasing SPS temperature. The iron-containing mixtures showed the formation of the iron carbide Fe_3C phase after the SPS. The degree of graphitization of porous materials obtained from the iron-containing compacts did not depend on the sintering temperature.

It was found that SPS of nanodiamonds in the presence of nickel leads to a dramatic decrease in the SSA of the carbon-based material. The presence of nickel enhanced the graphitization process and accelerated growth of the graphite crystallites. At the same time, it was not possible to detect any trend in the changes of the SSA of the carbon-based materials obtained after nickel has been dissolved from the Ni-C_{am} compacts. The SSA of the porous materials obtained from the Fe-C_{am} compacts remained practically unchanged in the compacts sintered at different temperatures. In the case of system Co-C_{am}, the SSA increases with increasing sintering temperature.

According to the Raman spectra and I_D/I_G of the samples, in which Ni and Co were used as graphitization catalysts, the graphitization degree increases with increasing sintering temperature. Increasing holding time did not enhance graphitization. The shape of the Raman spectra of the samples obtained from the Fe-C_{am} compacts shows little variation with the sintering temperature. From the presence of pronounced D-bands in the spectra, it can be concluded that the product of partial dissolution of iron from the compacts contained carbon that was poorly graphitized.

This work has shown that sintering of amorphous carbon and nanodiamonds in the presence of nickel or cobalt induces both graphitization and growth of graphite crystallites. Sintering of non-graphitic carbon in contact with iron presents a more complicated situation, in which it is not possible to transform carbon introduced into the initial mixture quantitatively into graphite due to the formation of the Fe_3C phase.

The formation of carbon nanotubes on the surface of diamond crystals catalyzed by nickel was investigated.

The results of the project have been presented in the following publications:

1. Multiwalled carbon nanotube forests grown on the surface of synthetic diamond crystals/ B.B. Bokhonov, A.V. Ukhina, D.V. Dudina, H. Katsui, T. Goto, H. Kato // Ceramics International 43 (2017) 10606–10609.
2. Structural characterization of carbon-based materials obtained by Spark Plasma Sintering of non-graphitic carbon with nickel and iron as catalysts and space holders/ A. V. Ukhina, B. B. Bokhonov, D. V. Dudina, K. Yubuta, H. Kato // Ceramic Transactions, 2017, accepted.
3. Morphological features of W- and Ni-containing coatings on diamond crystals and properties of diamond-copper composites obtained by Spark Plasma Sintering/ A. Ukhina,

B. Bokhonov, D. Samoshkin, S. Stankus, D. Dudina, E. Galashov, H. Katsui, T. Goto, H. Kato// Materials Today: Proceedings, 2017, accepted.
4. The influence of the formation of Fe_3C on graphitization in a carbon-rich iron-amorphous carbon mixture processed by Spark Plasma Sintering and annealing/ Dina V. Dudina, Arina V. Ukhina, Boris B. Bokhonov, Michail A. Korchagin, Natalia V. Bulina, Hidemi Kato// Ceramics International, 2017, accepted

Table 1. The fabrication conditions and characteristics of the carbon-based materials obtained by SPS of metal-carbon mixtures followed by selective dissolution of the metal: composition of the initial metal-carbon mixtures, sintering temperature and holding time, apparent density of the sintered metal-carbon compacts, specific surface area of the carbon based materials and I_D/I_G ratio of the corresponding Raman spectra of the carbon-based materials.

Metal-carbon powder mixture	SPS temperature, °C	Holding time, min	Apparent density, g·cm^{-3}	I_D/I_G	SSA, m^2/g
Ni-C_{nd}	800	3	4.94	0.86	240
Ni-C_{nd}	800	10	4.98	0.95	180
Ni-C_{nd}	1000	3	5.94	0.21	20
Ni-C_{am}	500	10	3.63	0.78	42
Ni-C_{am}	600	10	4.07	0.68	28
Ni-C_{am}	700	10	4.29	0.64	57
Ni-C_{am}	800	10	5.11	0.55	44
Ni-C_{am}	1000	10	5.22	0.31	16
Fe-C_{am}	600	5	3.28	0.85	51
Fe-C_{am}	800	5	3.33	0.84	57
Fe-C_{am}	900	5	3.77	0.90	55
Co-C_{am}	800	3	4,5	0.87	80
Co-C_{am}	1000	3	5,11	0.80	62

Keywords: catalytic, phase transformation, raman spectroscopy
Full Name: Arina Ukhina, Institute of Solid State Chemistry and Mechanochemistry, Siberian Branch of the Russian Academy of Sciences (SB RAS), Novosibirsk, Russian Federation
E-mail: auhina181@gmail.com

Characterization of Products of Competitive Reactions during Quenching and Partitioning Applied to a Ductile Cast Iron

Competitive reactions have been reported to occur during critical steps of the Quenching and Partitioning process, leading to very complex microstructures. In this work we have characterized the products of competitive reactions – namely transition carbides and bainitic ferrite – by SEM, EBSD, and 3D-APT. A methodology for determining the accurate orientation relationship between fcc and bcc phases has been successfully implemented.

The Quenching and Partitioning (Q&P) process applied to ductile cast irons has been proposed as an alternative heat treatment to obtain austenite-containing microstructures similar to those found in the austempered ductile cast iron (ADI) [1][2]. The Q&P process involves a partial quenching of the material to produce a controlled mixture of martensite (α') and untransformed austenite (γ), followed by a "partitioning" step, when the material is isothermally held at a higher temperature to promote the carbon diffusion from the carbon-supersaturated martensite to austenite. The carbon-enriched austenite is stabilized by the high carbon content and does not transform into martensite during the final cooling. In the final microstructure, martensite confers high strength, while stabilized austenite favors good ductility due to occurrence of TRIP effect [1][3]. Competitive reactions, such as carbides precipitation in martensite and decomposition of austenite to bainite, are reported to occur during the partitioning step, leading to very complex microstructures. Addition of large fractions alloying elements (e.g., Si and Mn) has been proposed to avoid such reactions, but processing difficulties (e.g., microsegregation) have been reported to arise from this practice [4].

A low Mn ductile cast iron alloy (Fe - 3.47C - 2.47Si - 0.20Mn - 0.38Cu, wt.%) was submitted to Q&P heat treatments at various conditions was previously characterized by SEM, EPMA, dilatometry, and in-situ synchrotron X-ray diffraction. Austenitization was carried out at 880 °C in the γ + graphite phases field and initial austenite carbon composition is approximately 0.8 wt.%. Formation of bainitic ferrite (α_b) was observed by in-situ XRD and has been pointed out as the main mechanism of austenite carbon-enrichment. Evidence of transition carbides precipitation was obtained by analysis of EPMA and in-situ XRD results. The aim of this collaborative work was to identify the critical heat treatment steps were carbides precipitation occurs, to understand the distribution of retained austenite and fresh martensite. To achieve this goal, experimental techniques performed at IMR encompassed SEM, EBSD, and 3D-APT.

SEM characterization shows presence of fine dispersion of carbides inside martensite plates after very short partitioning times (< 30 s), as shown in Fig. 1a. EBSD characterization reveals localized distribution of retained austenite after the Q&P heat treatment. For short partitioning times (Fig. 1b), large regions that did not transform into martensite or bainitic ferrite up to the end of the partitioning step transform into fresh martensite during the final cooling. Retained austenite is mainly observed surrounding martensite and bainitic ferrite plates/laths. Longer partitioning times (Fig. 1c-d) lead to a higher fraction of bainitic ferrite, and a more homogeneous distribution of austenite, while formation of fresh martensite is ceased.

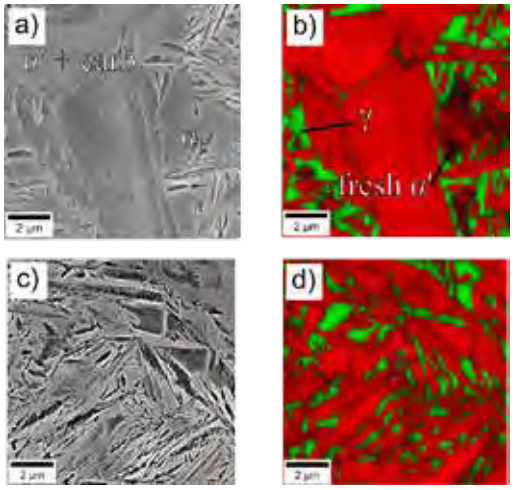

Fig. 1: SEM and EBSD phase maps of Q&P treated samples. Phase colored as red were indexed as bcc, while phase colored as green were indexed as fcc. a) and b): quenching at 170 °C, partitioning at 375 °C for 30 s. c) and d): quenching at 170 °C, partitioning at 375 °C for 15 min.

The microstructure of a sample partially quenched but not subjected to the partitioning step presents etching features that resemble carbides. 3D-APT characterization of the same sample (Fig. 2a-b) shows presence of carbon clusters achieving maximum carbon content of 15 at.%, much lower than the stoichiometric composition of cementite (25 at.%) or transition carbides (e.g., ε carbide, 25-33 at.%). From these results it is proposed that carbon clusters formed during the quenching step act as nucleation sites for precipitation of transition carbides during the reheating and partitioning steps of the Q&P heat treatment.

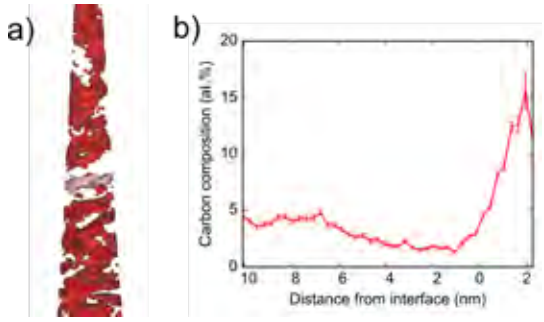

Fig. 2: 3D-APT analysis of sample quenched at 170 °C for 1 min then cooled to room temperature. a) Isoconcentration (4 at.%) surfaces of carbon composition. b) Carbon proxigram obtained on the volume highlighted in Fig. 2a.

Accurate orientation relationship between the bcc (martensite and bainitic ferrite) and the fcc (austenite) products was also determined from the measured EBSD data [5]. In Fig. 3a the deviation of the accurate orientation relationship from the Kurdjumov-Sachs orientation relationship (KS-OR) in a Q&P treated sample is represented in color map. Differences of deviation angle are observed inside single bcc microconstituents plates/laths. Fig. 3b shows the same information obtained for a material containing only bainitic ferrite and austenite (produced by austempering). The bainite product in this microstructure is coarser and the deviation of the accurate OR from the KS-OR is notably higher than in the Q&P sample. Since in the Q&P sample bainitic ferrite is nucleated at martensite/austenite interfaces, it is suggested that the martensite/austenite OR plays an important role defining the bainitic ferrite/austenite OR.

In summary, we have conducted extensive characterization work on Q&P multiphase microstructures. Valuable information about phase distribution was obtained by SEM and EBSD analysis. A methodology for determining the accurate orientation relationship between bcc and fcc phase has been successfully implemented for the current set of microstructures.

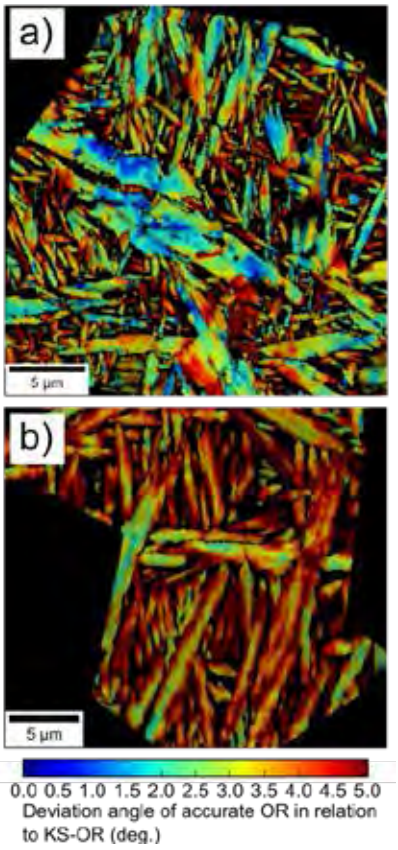

Fig. 3: Deviation angle of the measured accurate OR in relation to KS-OR. a) Sample austempered at 375 °C for 15 min ($\alpha_b + \gamma$ microstructure). b) Q&P sample quenched at 170 °C and partitioned at 375 ° for 30 s.

References

[1] J. G. Speer, D. V. Edmonds, F. C. Rizzo, and D. K. Matlock, Curr. Opin. Solid State Mater. Sci.,. 8, 219-237 (2004)
[2] A. J. S. T. Silva, H. Goldenstein, W. L. Guesser, M. F. Campos, Mat. Res., 17, 1115-1123 (2015)
[3] M. J. Santofimia, L. Zhao, and J. Sietsma, Metall. Mater. Trans. A, 40, 46-57 (2009)
[4] F. HajyAkbary, J. Sietsma, G. Miyamoto, T. Furuhara, and M. J. Santofimia, Acta Mater., 104, 72-83 (2016)
[5] G. Miyamoto, N. Takayama, and T. Furuhara, Scr. Mater., 60, 1113-1116 (2009)

Keywords: microstructure, high strength steel
Arthur Seiji Nishikawa (Department of Metallurgical and Materials Engineering, University of São Paulo, São Paulo, Brazil)
E-mail: arthur.nishikawa@usp.br
www.st-mat.imr.tohoku.ac.jp, pmt.usp.br/ltf

Geometrical Dependence of Magnetic Properties for Magnetic Antidot Lattices of Heusler Alloy

$Co_2Fe_{0.4}Mn_{0.6}Si$ Heusler alloy thin films with $L2_1$ ordered structure have been prepared using ultrahigh vacuum magnetron sputtering. Magnetic antidot lattice (MAL) arrays with square, circular, triangular, and diamond shaped holes with the feature size of 100 nm, 200 nm, and 500 nm have been microfabricated using e-beam lithography. Magneto-optical Kerr effect measurements using the micro-size laser spot, which is called μ-MOKE, revealed the appearance of strong cubic and weak uniaxial magnetic anisotropy in the Heusler alloy thin films.

Half-metallic Heusler compounds with full spin polarization have recently attracted huge research interest because of their potential applications in spintronic devices [1]. On the other hand, the magnetization reversal in magnetic antidot lattice (MAL) arrays is better controlled in comparison to continuous thin films because the well-defined periodic holes act as the nucleation and pinning centers for the reversed domains. The exchange coupled MAL arrays are ideal for ultrahigh density magnetic storage applications because of their physical dimension not being restricted by the superparamagnetic blocking [2]. The aim of this collaborative work is to understand the effect of shape and lattice geometry of the MAL arrays of Heusler alloy on the magnetization reversal and domain wall motion. Thin films with different thickness (15, 20, and 25 nm) were grown in an ultrahigh vacuum chamber with a base pressure < 1.5×10^{-7} Pascal. The epitaxial growth of the films was studied by x-ray diffraction (XRD). The MAL arrays with different shapes and lattice symmetries were microfabricated using e-beam lithography and subsequently Ar^+ ion milling. The magnetic hysteresis loops have been investigated by vibrating sample magnetometry (VSM) and magneto-optical Kerr effect system having the micro-size laser spot (μ-MOKE).

VSM measurements revealed highest saturation magnetization (M_s) and coercive field (H_c) for the Heusler alloy thin film with thickness of 20 nm. Fig. 1 shows the H_c vs ϕ (angle between applied magnetic field and easy magnetization axis) plot for the thin films measured using μ-MOKE. The plot reveals the formation of epitaxial growth induced the strong cubic anisotropy and the weak uniaxial anisotropy. The possible origin for the uniaxial anisotropy can be many viz. oblique angular deposition, strain relaxation, anisotropic formation of chemical bonds, interfacial roughness due to lattice mismatch, surface morphology, etc. Fig. 2 shows the scanning electron microscopy (SEM) images of the microfabricated MAL arrays of square, circular, triangular, and diamond shaped holes with the feature size of 500 nm. μ-MOKE measurements revealed magnetic hardening in the MAL arrays with incorporation of the holes in the continuous thin films. This is expected because the domain wall propagation in such MAL arrays is laterally restricted by the presence of the periodic holes.

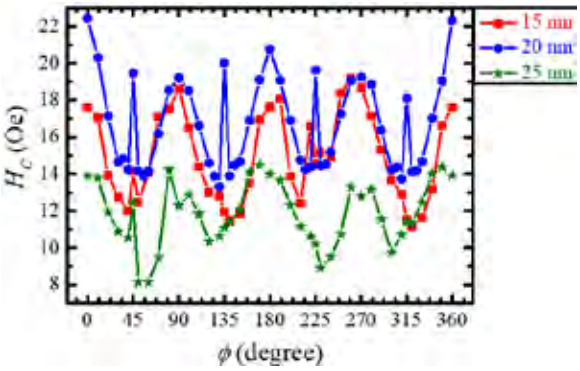

Fig. 1: H_C vs ϕ plot for Heusler alloy thin films with thickness of 15 nm (red curve), 20 nm (blue curve), and 25 nm (green curve).

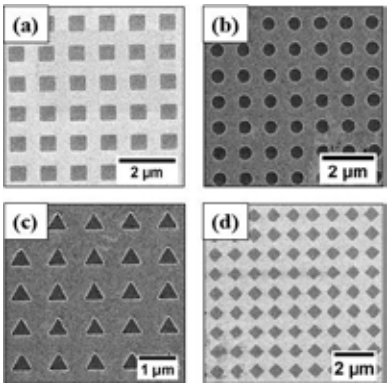

Fig. 2: SEM images of square (a), Circular (b), triangular (c), and diamond (d) shaped antidots with feature size of 500 nm.

The static and dynamic response of the magnetization and domain walls will be performed using Kerr microscope, time-resolved MOKE, magnetic force microscopy (MFM), and x-ray photoemission electron microscopy (XPEEM).

References

[1] T. Seki, Y. Sakuraba, H. Arai, M. Ueda, R. Okura, H. Imamura, and K. Takanashi, Appl. Phys. Lett. 105, 092406 (2014).

[2] S. Bedanta, and W. Kleemann, J. Phys. D: Appl. Phys. 42, 013001 (2009).

Keywords: half-metal, magnetic properties, lithography

Full Name: Sougata Mallick, National Institute of Science Education and Research (NISER), Bhubaneswar, India
E-mail: sougata.m@niser.ac.in
http://www.niser.ac.in

Antiferromagnetic anisotropy determination by spin Hall magnetoresistance

We propose an electric method for the antiferromagnetic anisotropy determination through spin Hall magnetoresistance (SMR) measurement in normal metal (NM)/antiferromagnetic insulator (AFI) bilayers. This work elaborates a new method for the antiferromagnetic anisotropy determination in both AFI bulk material and thin films.

Antiferromagnetic spintronics is an emerging research field since antiferromagnetic (AFM) materials have great potential for the spintronics applications, which has been demonstrated by recent experimental and theoretical progress [1,2]. At the same time, however, very limited effort has been made to utilize spintronics phenomena to characterize the magnetic property of AFM. In this work, we propose that the spin Hall magnetoresistance (SMR) in a normal metal (NM)/antiferromagnetic insulator (AFI) bilayer can be utilized to determine the antiferromagnetic anisotropy in the AFI.

In this paper, we simulated the SMR in realistic NM/AFI bilayer systems, such as Pt/Cr_2O_3, Pt/NiO and Pt/CoO. Our work shows that the SMR in a NM/AFI bilayer provides a new electric method for the antiferromagnetic anisotropy determination in both bulk material and thin films. Besides, the simulated SMR results in realistic system with uniaxial Cr_2O_3 and biaxial NiO, CoO yield a concrete reference for the experimental observation of the SMR in NM/AFI bilayers.

Figure 1(a) and (b) show the illustrations of the SMR in NM (NM=Pt)/AFI (AFI=Cr_2O_3, CoO, NiO) bilayer with AFI Néel vector $\boldsymbol{\Delta} = \mathbf{M}_A/M_A - \mathbf{M}_B/M_B$ parallel and perpendicular to the direction of the interface electron spin accumulation. In analogy to the SMR in NM/ferromagnetic insulator(FI) [3], in NM/AFI bilayers, when electron spin polarization $\boldsymbol{\sigma}$ and Néel vector $\boldsymbol{\Delta}$ are not parallel, spin-flip scattering is activated. Figure 1(b) shows when $\boldsymbol{\sigma} \perp \boldsymbol{\Delta}$, the spin-transfer torque induced absorption at the NM/AFI interface will be maximized, which gives a higher resistance than the state $\boldsymbol{\sigma} \parallel \boldsymbol{\Delta}$.

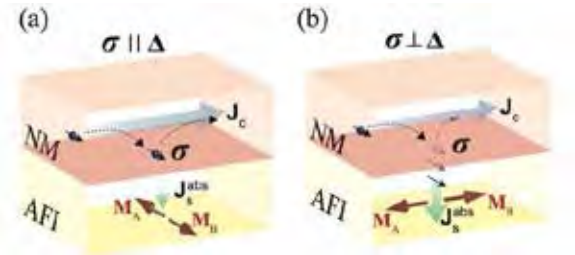

Fig. 1 (a), (b) Illustrations of the SMR in NM (NM=Pt)/AFI (AFI=Cr_2O_3, CoO, NiO) bilayer with AFI Néel vector parallel and perpendicular to the direction of the interface electron spin accumulation. $\mathbf{J}_C$ and $\mathbf{J}_S^{abs}$ represent the injected charge current and the spin current absorption in AFI respectively. $\mathbf{M}_A$ and $\mathbf{M}_B$ are the AFI sublattices.

In an AFM material, the Néel vector $\boldsymbol{\Delta}$ will stay along the easy axis below the Néel temperature due to the anisotropy. When applying magnetic field $\mathbf{H}$ parallel to the easy axis with magnitude larger than the critical field H_C, the Néel vector will suddenly changes its direction perpendicular to $\mathbf{H}$, this first-order transition is called spin-flop transition. Since in general cases, the Néel vector in AFM is determined by both the external magnetic field and the magnetic anisotropy [4]. Combining the angular dependence of the Néel vector with the SMR in NM/AFI, we simulated the angular dependence of the SMR in Pt/ Cr_2O_3 (110) bilayers with different magnetic fields, as shown in Fig. 2.

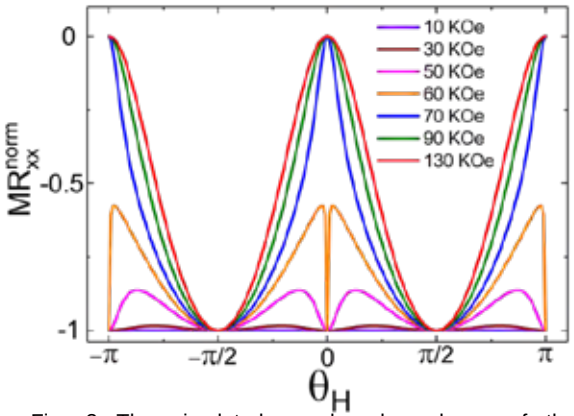

Fig. 2 The simulated angular dependence of the normalized SMR resistivity in Pt/ Cr_2O_3 (110) with different magnetic fields. θ_H is the angle between the magnetic field $\mathbf{H}$ and easy aixs.

In conclusion, we propose a new method for the antiferromagnetic anisotropy determination in both AFI bulk material and thin films through SMR measurement in NM/AFI bilayers.

References

[1] T. Jungwirth, X. Marti, P. Wadley and J. Wunderlich, Nat. Nanotech. 11, 231 (2016).

[2] S. Seki, T. Ideue, M. Kubota, Y. Kozuka, R. Takagi, M. Nakamura, Y. Kaneko, M. Kawasaki and Y. Tokura, Phys. Rev. Lett. 115, 266601 (2015).

[3] H. Nakayama, M. Althammer, Y. T. Chen, K. Uchida, Y. Kajiwara, D. Kikuchi, T. Ohtani, S. Geprägs, M. Opel and S. Takahashi, R. Gross, G. E. W. Bauer, S. T. B. Goennenwein and E. Saitoh, Phys. Rev. Lett. 110, 206601 (2013).

[4] T. Nagamiya, K. Yosida and R. Kubo, Advances in Physics 4, 1 (1955).

Keywords: spintronic, magnetoresistance

Full Name: Hua Wang, Dazhi Hou, Zhiyong Qiu, Takashi Kikkawa, Xiaofeng Jin, Eiji Saitoh
E-mail: huawang@imr.tohoku.ac.jp

Multiferrocity in the Gapless Quantum Antiferromagnet NH_4CuCl_3

We have developed a ESR and a magnetization probes in which a high electric field can be applied in addition to a high magnetic field. The highest voltage is about 1000 V at 4.2 K. It was enabled by the use of multiple thin polyimide tubes for electrode cover. At low temperatures, the voltage effect is not obvious, presumably because the barrier is too large to switch the polarization in the electric field of 1000 V.

Multiferroics compounds that can simultaneously exhibit long range magnetic and dielectric orders, have been the subject of intense study over the past decade. One reason is their great potential for a variety of practical applications, which includes data storage devices, data encryption, microwave devices, ac field sensors, transducers, actuators and more. Unfortunately, a number of fundamental physical restraints has resulted in a paucity of such materials, requiring a different approach to their synthesis and discovery.

One of the important question is the coupling between the magnetic and the electric orders. Also the coupling between the responses to the magnetic and the electric fields. The purpose of this project is to establish the experimental methods to measure the magnetization and the ESR under the coexisting of two kinds of fields-magnetic and electric fields.

As the target for this research, a new class of multiferroics, NH_4CuCl_3 is chosen. It is the three dimensionally coupled S=1/2 spin dimer system. The zero field ground state is gap-less and there are 1/4 and 3/4 magnetization plateau for the macroscopic quantization of the magnetization. For this compound, dielectric, specific heat, mass spectroscopy and X-ray measurements, ESR and other properties have been investigated. To date, there is no investigation of ESR in the presence of the electric field.

Figure 1 shows the schematic drawing of the sample mount in ESR probe in electric field. The sample is mounted on the polyethylene sample case with the bottom and top electrodes. The bottom one is connected to the light pipe made of SUS304 and then to the electric ground. The top one is connected to the high voltage electrode from the high voltage power supply. The sample is sealed into the stainless pipe with He-exchange gas. In the diluted He gas, the discharge takes place in the relatively low

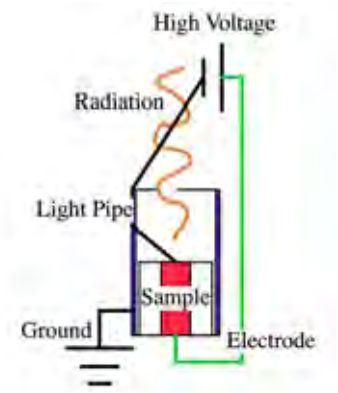

Fig. 1 Schematic diagram of ESR setup.

voltage threshold of several hundreds volt. On the other hand, the thick cover on the high voltage line results in the high loss in the transmission of the electromagnetic wave. In the present system, we have used an ultra-thin polyimide tubes in the range of 0.1-0.6 mm in diameter. By putting those tubes with sufficient overlap, we could apply the high voltage as high as 1000 V to the sample.

We have measured at several frequencies to observe different ESR modes. At 190 GHz, we can observe the ground state ESR signal and the excitation from the singlet to triplet states. By allying the high voltage keeping the sample at 1.7 K, we see a small change of the base line, but there is no large change in the ESR spectrum. It may show the large barrier to modify the ferroelectric order in low temperatures.

We have also succeeded in applying the high voltage in the magnetization measurement specimen. However, the magnetization signal was weak for the used small sample with the diameter of 0.2 mm. A sufficient signal can be obtained by using the larger sample.

In summary, we have succeeded in the application of high voltage in the high frequency ESR and high field magnetization. The further investigation of the magnetic properties of NH_4CuCl_3 is in progress.

Keywords: multiferroic, high magnetic field
Dr. J. Kinyon, Florida State University and H. Nojiri, IMR, Tohoku University
E-mail: nojiri@imr.tohoku.ac.jp
http://www.hfpm.tohoku.ac.jp

Porous Co-Cr Alloy Fabricated by LMD (Liquid Metal Dealloying) Process

Nowadays, Co-Cr alloy has been applied on bio-medical applications such as implants due to its high biocompatibility as well as excellent mechanical properties [1]. Especially, biocompatibility of implant materials can be enhanced drastically if it is processed into porous structure. In this work, we tried to introduce pores on Co-Cr alloy matrix by liquid metal dealloying (LMD) process.

Liquid metal dealloying (LMD) process has received lots of interest nowadays [2]. LMD is a technique to fabricate porous structure by dealloying material with metallic melt instead of chemical etchant. To apply this process, a well-designed alloy system needs to be prepared in consideration of the heat of mixing (ΔH_{mix}) correlation.

To obtain Co-Cr alloy foam, first of all, we choose Ca as metallic melt material of LMD process, since it exhibits not only high biocompatibility, but also bio-degradability. Moreover, we prepared a Co-Cr-Ni ternary alloy as a precursor of LMD process. Here, only Ni shows large negative ΔH_{mix} with Ca. Which means that if we immerse this precursor into Ca melt with high temperature, only Ni is more likely to react and swap its position with Ca.

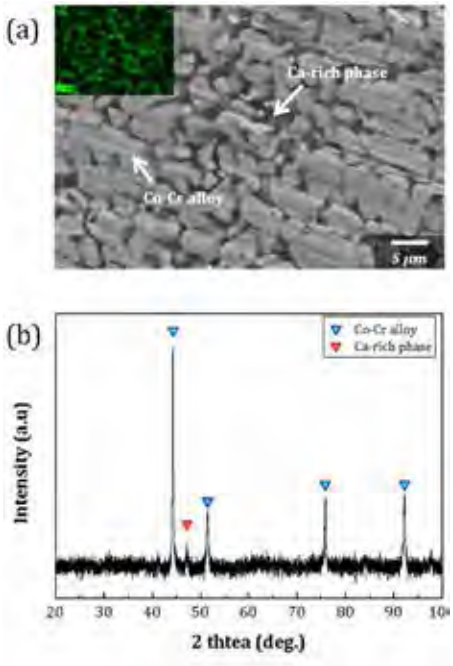

Fig. 1 (a) Microstructure of bi-continuous composite of Ca and Co-Cr alloy fabricated by LMD process and (b) X-ray scan of it.

Fig 1. shows the morphology of the bi-continuous structure of Ca and remained Co-Cr alloy after immersing the precursor in Ca melt. As we can see in EDS mapping image of Ca in (a), Ca is successfully separated with Co-Cr alloy. And this separation behavior can be also found with (b) XRD scan of this composite.

Co-Cr alloy foam was fabricated by leaching all the Ca phase out. Since Ca react with water actively, we immersed this precursor in deionized water for 24 hrs. and cultured osteoblast on Co-Cr alloy with pores.

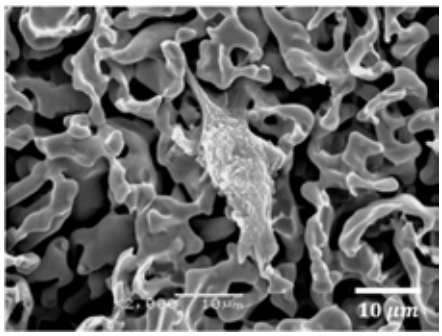

Fig. 2 Cultured cells on porous Co-Cr alloy fabricated by liquid metal dealloying process

As we can see in fig. 2, the Ca-rich phase is successfully dissolved and only Co-Cr alloy ligaments are remained. Moreover, the cells are well attached on each ligament.

Through this research, we fabricated Co-Cr alloy foam which was impossible to be formed by the chemical dealloying process. And we investigated its biocompatibility by attaching osteoblast on the foam. And this attempts will make an important progress of one step forward in bio-medical materials research.

References

[1] L. Shi, D. Northwood and Z. Cao, J. Mat. Sci. 28, Issue 5 (1993)
[2] T. Wada, K. Yubuta, A. Inoue and H. Kato, Mat. Lett. 65, Issue 7 (2011)

Keywords: Metal & Biomedical
Gukno, Yun (Department of materials science and engineering, Seoul national university)
E-mail: ykn2002@snu.ac.kr
http://espark.snu.ac.kr

Event

SMS2016

Summit of Materials Science 2016 (SMS2016)
Chairperson K. Takanashi (IMR)

The Summit of Materials Science (SMS) is an international forum, held by the IMR and initiated after the catastrophic earthquake in 2011. It covers a broad range of topics in solid-state physics and chemistry, as well as materials science. This time, SMS 2016 was organized as a part of our centennial celebration. It started by the opening speech, entitled "Past and Present of IMR", by the director Koki Takanashi, which was followed by 25 invited talks, on Spintronics, Magnetism, Crystal Growth, Energy-related Materials, Structural Alloys and Ceramics, Phase Transformation, etc. Immediately prior to this forum, a Young Scientist Workshop was held. 18 oral and 64 poster presentations were given in English by burgeoning researchers from the institute. The central objective of this meeting was, along with scientific interactions, to exchange opinions and discuss the future of materials science. Under the motto "My Dream, My Ambition", every presentation radiated uplifting enthusiasm. In this way, SMS 2016, with 166 participants including 48 from overseas, contributed a memorable milestone to the history of IMR.

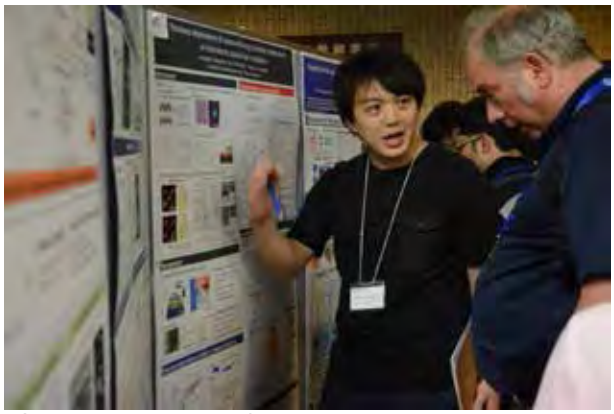

Photo1: Poster Session
Photo2: SMS conference

Photo3: Commemorative photograph at the SMS2016

ICC-IMR FY2016
Activity Report

Edited by ICC-IMR Office
Published in February, 2018

Contact: International Collaboration Center,
Institute for Materials Research (ICC-IMR)
Tohoku University
2-1-1, Aoba-ku, Sendai, 980-8577, Japan
TEL&FAX: 81-22-215-2019
E-mail: icc-imr@imr.tohoku.ac.jp

Printing: HOKUTO Corporation

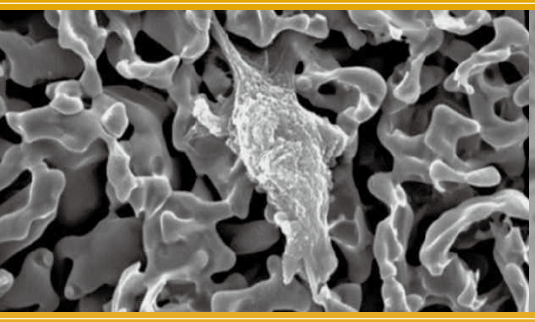

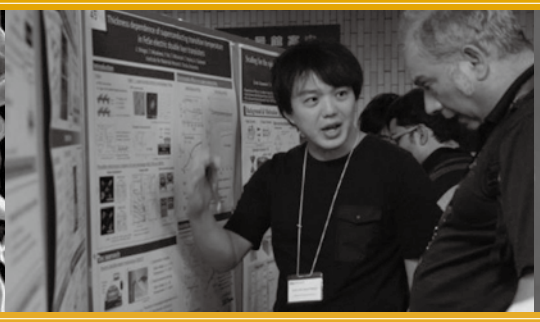

この冊子は「水なし印刷」により印刷しております。

環境にやさしい植物油インキ「VEGETABLE OIL INK」で印刷しております。